A principled approach to community detection in interareal cortical networks

Jorge Martinez Armas[a], Kenneth Knoblauch[b,c], Henry Kennedy[b,d,e], Zoltan Toroczkai[a,1]

[a]Department of Physics University of Notre Dame, Notre Dame, IN 46556, USA;
[b]Univ Lyon, Université Claude Bernard Lyon 1, INSERM, Stem Cell and Brain Research Institute U1208, 69500 Bron, France;
[c]National Centre for Optics, Vision and Eye Care, Faculty of Health and Social Sciences, University of South-Eastern Norway, Kongsberg, Norway
[d]Institute of Neuroscience, Center for Excellence in Brain Science and Intelligence Technology, Chinese Academy of Sciences, Shanghai 200031, China;
[e]Shanghai Center for Brain Science and Brain-Inspired Intelligence Technology, Shanghai 200031, China;

[1]To whom correspondence may be addressed. Email: toro@nd.edu

ORCIDs:
J.M.A.: https://orcid.org/0000-0002-9758-967X ;
K.K.: https://orcid.org/0000-0002-4681-4638 ;
H.K.: https://orcid.org/0000-0002-2796-7663 ;
Z.T.: https://orcid.org/0000-0002-6602-2849 ;

This PDF file includes:
Main Text (7183 words)
Figures 1 to 6
Methods (3840)
References (75)

Extended Data contains Figures 1 to 8, Tables 1

Abstract 146/150wds

Structural connectivity between cortical areas, as revealed by tract-tracing is in the form of highly dense, weighted, directed, and spatially embedded complex networks. Extracting the community structure of these networks and aligning them with brain function is challenging, as most methods use local density measures, best suited for sparse graphs. Here we introduce a principled approach, based on distinguishability of connectivity profiles using the Hellinger distance, which is relatable to function. Applying it to tract-tracing data in the macaque, we show that the cortex at the interareal level is organized into a hierarchy of link-communities alongside with a node-community hierarchy. We find that the ½-Rényi divergence of connection profiles, a non-linear transform of the Hellinger metric, follows a Weibull-like distribution and scales linearly with the interareal distances, a quantitative expression between functional organization and cortical geometry. We discuss the relationship with the extensively studied SLN-based hierarchy.

How the brain works is an inverse problem, namely, using observational data to back-engineer functionality and principles of information processing. As the brain is a complex networked system, one approach is to study this network and how its structure deviates from that of other, random networks, serving as null models. The deviations and their heterogeneity across scales reflect structural and functional specificities of the brain (Sporns, Tononi and Kötter, 2005; Bullmore and Sporns, 2009; He and Evans, 2010; Bassett and Sporns, 2017; Váša and Mišić, 2022).

A heavily used approach in studying a network's structural organization is identifying its communities (Fortunato, 2010). In their original definition, communities (or clusters) are subsets of nodes that are more interconnected amongst themselves than with the rest of the network. A more general definition, which we also adopt, considers communities to be subsets of network objects (nodes, edges, subgraphs, etc.) that are "closer" to one another by some pre-defined measure, called similarity measure, than to the rest of the network. When the "network objects" are themselves communities, we are dealing with communities of communities, that is, a hierarchical organization of the network (Ravasz *et al.*, 2002; Clauset, Moore and Newman, 2008; Ravasz, 2009; Nikola T. Markov *et al.*, 2014; Harris *et al.*, 2019).

A large body of network literature shows that communities in networked systems are associated with components that perform specific functions (Strong, Lawton and Southwood, 1984; Mesulam, 1990; Fortunato, 2010; Ruan, Dean and Zhang, 2010; Onnela *et al.*, 2012; Li and Pang, 2013; Henry *et al.*, 2016). This is related to the fact that heterogeneous structures have a much larger capacity to encode information or perform a more diverse set of functions, than homogeneous structures, the latter having no community structure (other than the trivial one). Therefore, one would also expect the same property to hold for neuronal networks, which is indeed the case, as the tight relationship between network communities and function in the brain is a well-documented observation (Wu *et al.*, 2011; Sporns, 2013; Pessoa, 2014; Sporns and Betzel, 2016). Since information in the brain is encoded by the activities of neuronal populations (Buzsáki, 2010), the structure of the network plays a crucial role in the specificity and tunability of the activities of those populations (Michalareas *et al.*, 2016; Vezoli *et al.*, 2021). The principal manner in which a network (that performs a set of functions) differs from a homogeneous random network is through the existence of communities, which we posit, form a key organizational feature, reflective of the way information is processed in the brain. Moreover, we hypothesize that this property holds across all scales in the brain, including at the mesoscale, working with functional areas as network nodes and physical connectivity in form of axonal bundles as network links, forming the interareal network.

Here we present a novel method for analyzing the community structure of neuronal networks to help better understand the role of the connections and their weights (axon bundle densities) in shaping the network's functions. We focus on the mesoscale, i.e., on the interareal network, given the datasets available to us, but the methodology we develop is applicable at any scale. Due to the nature of the interareal network, which is a dense, directed and weighted graph, most state-of-the-art algorithms are unsuitable since they rely on optimizing communities using modularity-like approaches (Newman, 2004; Palla *et al.*, 2005; Rosvall, Axelsson and Bergstrom, 2009; Ahn, Bagrow and Lehmann, 2010a; Bodlaj and Batagelj, 2015), which are inappropriate in dense graphs. Moreover, instead of using ad-hoc measures (usually borrowed from social network analysis) we want to develop a principled approach, where we choose our criteria for community definition related to the roles performed by these structures; thus, expectedly, the communities and the hierarchies obtained should be a direct reflection of how information processing is organized in the brain. It is important to mention that community detection does not provide a unique decomposition of the network into subgraphs, as it is strongly dependent on the

definition of the similarity measure and on the community merging criteria. For example, in a social network, communities obtained by physical co-location (families) are not the same as those obtained by work interactions (organizations).

Our approach to community detection in neuronal networks is based on first finding the communities formed by the links/edges (Ahn, Bagrow and Lehmann, 2010b), then using that to generate the node-communities and capture their hierarchical organization (if any). The reason for this is because links connecting similarly structured network neighborhoods will have similar roles, given that in the brain, the network structure is a major part of the algorithm itself (Horvát *et al.*, 2016; Laydevant *et al.*, 2024; Molnár *et al.*, 2024), as argued in the paragraph above. Starting from link communities is also advantageous, because usually there are many more links than nodes, especially true for brain neuronal networks at the areal level, those being highly dense structures. In the macaque dataset studied here the edge-complete part (see Glossary in the Methods section) of the network has only 40 nodes but 999 directed edges. The community structure within the larger sized link data thus provides significantly more information than at the nodal level, although it is also more difficult to interpret. This is an issue with link-community detection, namely, interpretability, resulting in a reduced popularity, compared to the node-based community detection algorithms.

There is an interesting link-community study by de Reus et al. (de Reus *et al.*, 2014) performed on white matter pathways data in the human connectome, obtained with dMRI. The network is treated at the binary (unweighted) level, using undirected line-graph modularity optimization methods but the study does not identify node communities nor hierarchies (of neither type, link- or node- based), and it is different in scope from the present work. An interesting paper by Meunier et al. (Meunier, Lambiotte and Bullmore, 2010) presents hierarchical decomposition of human brain functional networks, based on functional magnetic resonance imaging datasets, showing that these activity-association based networks are organized in a hierarchically modular fashion. However, this does not imply anything directly about the hierarchical organization of the physical/anatomical network itself, but it provides an indirect support to the observations presented here.

After generating the link-communities at all levels and their hierarchical organization, we show how we can use that information in a principled way, to generate the node communities and their hierarchy. This is natural, because nodes and node communities interact through network links and thus the link-community structure will induce a partitioning of the nodes into groups. Interestingly, this approach, however, has not yet been proposed in the network literature, to our best knowledge. The standard and well-known link-community detection algorithm was introduced by Ahn, Bagrow and Lehmann (ABL) in 2010 (Ahn, Bagrow and Lehmann, 2010a), which we rely upon, in this work. However, it needs to be modified, using a different similarity measure than the one used in ABL, which was based on local network density. The modification is necessary, because local density measures do not give a sufficiently contrasting signal in networks that are already dense, such as the interareal cortical networks found in rodents and non-human primates (N. T. Markov *et al.*, 2014; Horvát *et al.*, 2016; Gămănuţ *et al.*, 2018).

The article is organized as follows. We first discuss the principles behind our definition of node and link similarity in neuronal networks and introduce a novel dissimilarity measure based on the so-called Hellinger distance (Hellinger, 1909; Cam and Yang, 2000), a measure of distinguishability of two probability distributions. This also allows us to make a connection with an information theoretic measure, the ½-Rényi divergence $D_{1/2}$, related to the Hellinger distance via a non-linear transformation, providing an explicit relationship between the geometrical organization of the neuronal network and its functional properties. Note, our approach is generally applicable to all spatial networks (including from other fields) in which link weights have a probabilistic

interpretation. Next, we generate the link-community hierarchy using the ABL algorithm with the modified similarity measure and compare it to a randomized version of the same network (null-model). This will show that there is a significant amount of structural heterogeneity and specificity in the original network data, at the level of link communities. We also compare it to the case where we use shortest physical distances between areas' barycenters through the white matter (Ercsey-Ravasz *et al.*, 2013) as a (dis)similarity measure and discuss the differences. We then present the principles behind our method for community extraction at the nodal level, from the link-community structure, resulting in the node-level community hierarchy of the macaque, as one of our main results. We continue with a method that selects the optimal level of the node-community hierarchy and discuss its properties. Finally, we discuss the relationship of our node-community hierarchy with the SLN-based hierarchy, a well-studied organization of the visual system, using the feedforward (FF) and feedback (FB) classification of connections.

Results

A network interpretation of function

In order to develop our community detection method, we first discuss the notion of function. Despite the fact that it plays a critical role in biology, sociology, etc., "function" is not easily quantifiable. Function within a biological (or sociological) system implies some kind of systematic organization, so that the dynamics that runs through the system has usually a well-defined and repeatable outcome and thus function is connected to the notion of order. While we can quantify disorder with various notions of entropy, we do not have a systematic quantification of order, as it can be of many different types; some networks may look rather random, while in fact they are ordered structures performing a multitude of functions. Here we propose a more practical treatment of the notion of function and functionality. The observation we are making is that function is not solely an attribute of an object or a system. It is instead, a *relationship* attribute, that is of the interactions between two or more objects or systems. Consider, for example, the myoglobin molecule. It binds, stores and releases an oxygen molecule, which by itself is a pointless/useless property. However, it becomes highly beneficial in oxygen storage and transport in the mammalian muscle tissue. In other words, myoglobin attains its function, via its interactions with muscle tissue. Note, that when specifying this function, we use the sequence: myoglobin → regulation of O_2 and NO → muscle tissue contraction (Kamga, Krishnamurthy and Shiva, 2012). Using network language, we propose that function is a property of an ordered pair of nodes (i, j), or equivalently, that node i performs a function towards node j. Regarding nodes as input/output units, the activity of node i towards node j serves as the input for the activity of j. In the brain, this is information or influence transfer (modulation). For our purposes, we quantify the functional output of a node i in the network by the list of its outgoing connections and their properties, i.e. by its out-link profile. In the brain we assume that all connections have a sustained role/function (otherwise they would not likely exist). Thus, the properties of the network of interareal connections are a direct reflection of the functional organization of the brain at the areal (mesoscopic) level. The links transfer information or modulation, which change the state of the receiving (downstream) nodes, which in turn modulates/changes their output downstream towards other nodes, etc.

Function is composable, in the sense that the union of activities of groups of nodes towards the rest of the nodes represents another function, possibly more complex/simple, depending on the higher/lower degree of connectivity of that group with the rest of the network. This composability property allows us to track the function-based hierarchy of the cortical network. While this network interpretation of function does not provide a translation

between connectivity and behavior (which would require characterization of the nodal states and their dynamics), it is a self-consistent approach, and on a structure whose properties can be analyzed/quantified and even compared across species, if a mapping can be made between the sets of nodes of the neuronal networks of the two species.

Link similarity

As mentioned previously, the clusters found in community detection reflect the network's organization from the point of view of the clustering criteria used. The criteria are formulated via a similarity measure, which allows us to decide if two network elements (nodes, links, subgraphs) belong to the same cluster (i.e., they are more similar) or not. Thus, if we want to understand how function is organized in the interareal network, our criteria and thus our similarity measure have to be brain function based. Since links

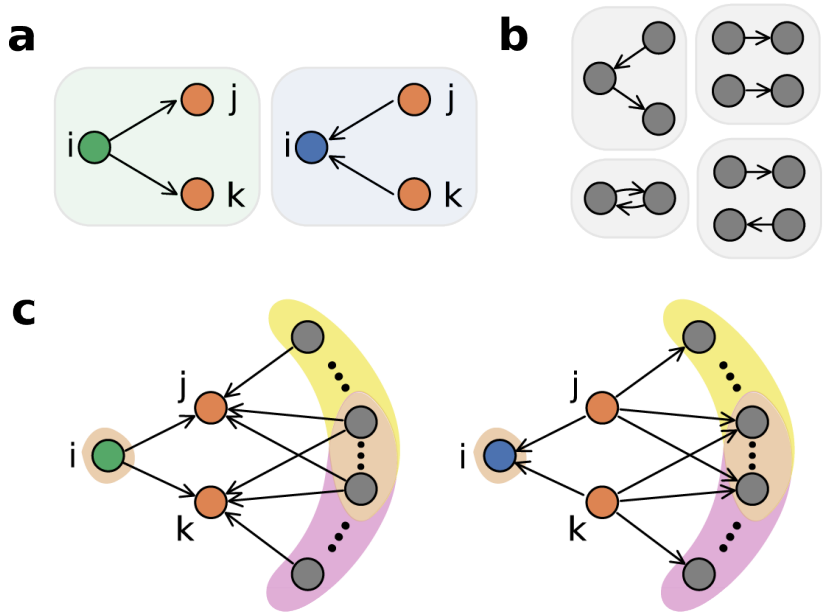

Fig. 1 | Defining the link similarity measure. a, Neighbor links have either a common start-node for out-links or a common end-node for in-links. **b**, All other pairs of links are disjoint. **c**, Similarity between two neighbor links is determined by the overlap between their weighted connectivity profiles of their non-common nodes j and k, using the Hellinger distance (see Methods section).

represent function as discussed above, one needs to define a similarity or distance measure between the links themselves. Directed *neighbor links* share either a common starting node but different end-nodes (referred to as out-neighbor links) or share a common end-node but different starting nodes (in-neighbor links). **Fig. 1**a shows two neighbor out-links (i, j) and (i, k), and two neighbor in-links (j, i) and (k, i). All other pairs of links are disjoint, see **Fig. 1**b. Only neighbor links can have non-zero similarity; disjointed links have zero similarity. We define the amount of similarity between two neighbor links by the *node-similarity* of their un-common nodes (j and k). In turn, we define the similarity of two nodes (j and k) via the overlap between their connectivity profiles, i.e., as given by all their weighted connections (which includes connections from/to the common node i), see **Fig. 1**c. In other words, the two out-going (in-coming) neighbor links' similarity is determined by the node-similarity of their end (start) nodes.

The Hellinger distance as a connection distinguishability measure

To define the similarity of two nodes we use a statistical distance measure, called the Hellinger distance (Hellinger, 1909). The Hellinger distance $H(P,Q)$, used for example in nonparametric density estimation, is a measure of the dissimilarity of two probability distributions P and Q, see the Methods section for details. For our purposes it has several advantages: *i)* it is a true metric, i.e., it is non-negative, symmetric, obeys the triangle inequality, that is $H(P,Q) + H(Q,R) \geq H(P,R)$, for any P,Q,R probability distributions, *ii)* it is a bounded metric with $0 \leq H(P,Q) \leq 1$, for any P,Q and *iii)* it relates to a practical statistical measure, called *sample complexity* $\mathcal{N}^{\delta}(P,Q)$. An important consequence of properties *i)* and *ii)* is mathematical consistency for comparisons. For example, if distributions P and Q are far but Q and R are close, then it follows that P and R are also far - a property that is not guaranteed to hold in general for similarity measures used in the literature. In our case, we use the Fraction of Labeled Neurons (FLN) as probability distributions, which are the link weights in the interareal network datasets. These are obtained via consistent retrograde tract-tracing injections into the cortex, see the Methods section for data description. Paper (Markov, Mária Ercsey-Ravasz, *et al.*, 2013) shows that the FLN weights admit a probabilistic interpretation so that the Hellinger distance is a good dissimilarity measure to use in the context of the brain. As a similarity measure, we use $S(P,Q) = 1 - H^2(P,Q)$, also called *affinity* or the Battacharyya coefficient (Bhattacharyya, 1946) (clearly $0 \leq S(P,Q) \leq 1$). By definition, disjoint links have the largest possible distance ($H = 1$) and thus lowest similarity value ($S = 0$).

The Hellinger distance is directly connected to the notion of sample complexity (Canonne *et al.*, 2019) which is a measure of how many times we need to sample from one probability distribution to tell them apart (Methods section). The smaller the Hellinger distance, the more samples are needed.

Fig. 2a shows H_{-}^2 and H_{+}^2 for all node pairs as function of white-matter interareal distances measured between the barycenters of each area (see Methods Section on information about these distances) for the nodes within the edge-complete network (ECN). One can see another advantage of using the Hellinger distance as dissimilarity measure: it is sensitive at all scales, especially at short distances, providing a good resolution in discernibility, also locally.

Rényi divergence of node-connectivity profiles

There is an interesting information-theoretic connection between the Hellinger distance and the α-Rényi divergence (Renyi, 1961), which is a generalization of the Kullback-Leibler divergence. Namely, for $\alpha = 1/2$, the ½-Rényi divergence $D_{1/2}$ (see the Methods section for its mathematical definition in terms of distributions P and Q) is connected to the Hellinger distance via the nonlinear relationship:

$$D_{1/2} = -2\log(1 - H^2) = -2\log S\,, \tag{1}$$

(note, $\alpha = 1$ is the classic Kullback-Leibler divergence) (Nielsen and Boltz, 2011). For our purposes, the ½-Rényi divergence has two main advantages: firstly, it is symmetric (unlike the Kullback-Leibler divergence) and secondly, it can handle zero values for any of the probability distributions, without going to infinity. One simple interpretation of the ½-Rényi divergence $D_{1/2}(P \parallel Q)$ is that is quantifies the error incurred when replacing the distribution P with distribution Q, assuming that the true distribution is P. It has a large number of applications in information theory, hypothesis testing, multiple source adaptation, coding and machine learning through approximate inference (Csiszar, 1995;

Morales, Pardo and Vajda, 2000; Mansour, Mohri and Rostamizadeh, 2009; Shayevitz, 2011; van Erven and Harremos, 2014; Li and Turner, 2016).

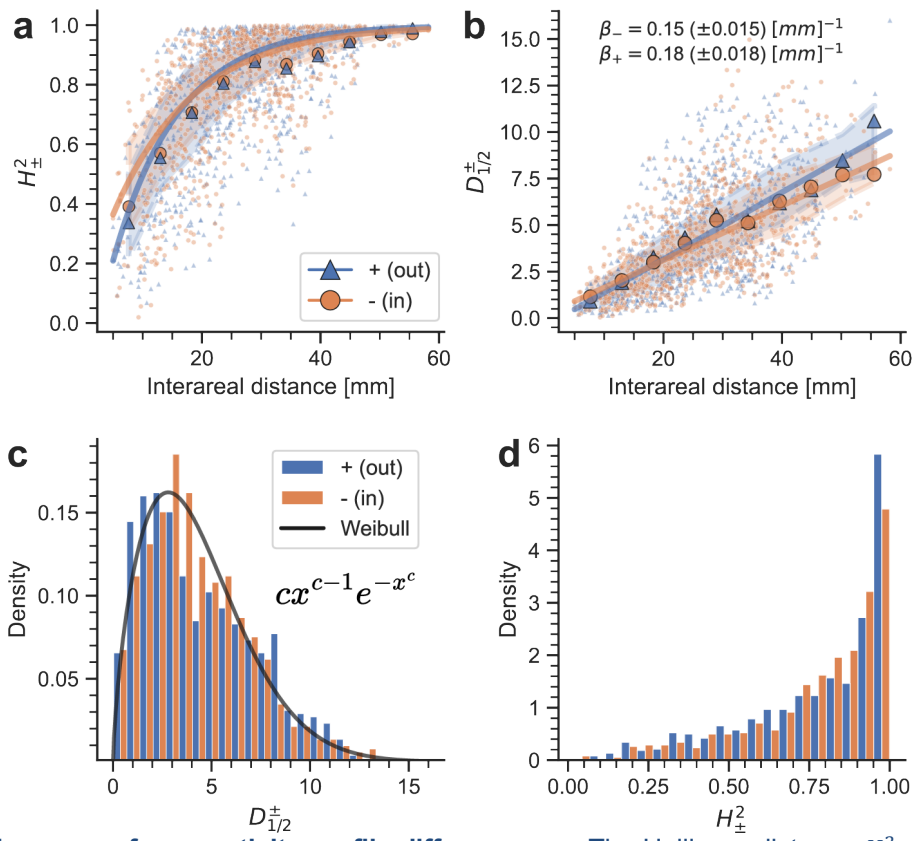

Fig. 2 | Measures of connectivity profile differences. a, The Hellinger distance $H^2_\pm$ as function of interareal distance for the macaque dataset. Lines, 95% confidence level (CL) uncertainty bands, and bin averages (large markers) are derived from the linear fits in panel **b,** using equation (1). **b**, ½-Rényi divergence, an information geometric measure as function of distance, showing a linear relationship. Lines and 95% CL uncertainty bands are obtained from a weighted linear regression from ten binarized averages and inverse variance weights. Slope regression coefficients $\beta_\mp$ ($\pm$ 95% CL) are shown at the top. **c**, The distributions of $D^\pm_{1/2}$ (bars) are well approximated with a Weibull distribution of shape and scale parameters $c = 1.67$ and $\sigma = 4.75$. **d**, histograms of $H^2_\pm$.

For example, consider two sensors with the same sampling rate, monitoring the occurrence of some phenomenon in a noisy environment. $D_{1/2}$ in this case provides a lower bound on the worst-case misdetection rate of the phenomenon (Shayevitz, 2011).

Plotting the $D^\pm_{1/2}$ values for all ordered area pairs as function of their distance, we obtain the plot in **Fig. 2**b. Interestingly, this shows an almost linear relationship between the Rényi divergence and interareal separation, with slightly different slopes. However, the scatter plot is heteroskedastic and there is significant variability for $D^\pm_{1/2}$ around the average, containing additional information. Histogram plots of $D^\pm_{1/2}$ exhibit unimodal distribution with fast decaying tails (see **Fig. 2**c). The continuous line is a fit of the Weibull distribution $f(y) = c\, y^{c-1} e^{-y^c}$ to the standardized data $y = (x - x_{\min})/\sigma$ where $x_{\min}$ is the minimum value of x (in our case $D^\pm_{1/2}$). c and σ are called the shape and scale parameters and fitting

gives $c = 1.67$ (or about $5/3$) and $\sigma = 4.75$ for our macaque dataset. In the Discussions section we will provide for $D^{\pm}_{1/2}$ being a Weibull distribution (a distribution from extreme value statistics) (Montgomery, 2020). **Fig. 2**d shows the histograms of $H^2_{\pm}$ for the macaque, a monotonically increasing function, indicating that the number of area pairs with a certain amount of dissimilarity between their connectivity profiles increases with their dissimilarity, and thus results in improved statistics, an advantageous feature.

The link-community hierarchy of the macaque cortex

Having defined a proper distance (or similarity) measure between the links as described above, we can now use the link-community detection algorithm (Ahn, Bagrow and Lehmann, 2010a) on the ECN of the macaque interareal network dataset. In brief, the link-community algorithm works as follows. At start, each link forms its own community, and we set the link community merging threshold value th at $th = 0$. We define the distance between two LCs C_i and C_j, $d(C_i C_j)$, as the minimum distance (in terms of either H^2_{+} and H^2_{-}) over all pairs of links, one from C_i the other from C_j, called *single-linkage criterion* in the literature (Müllner, 2013).

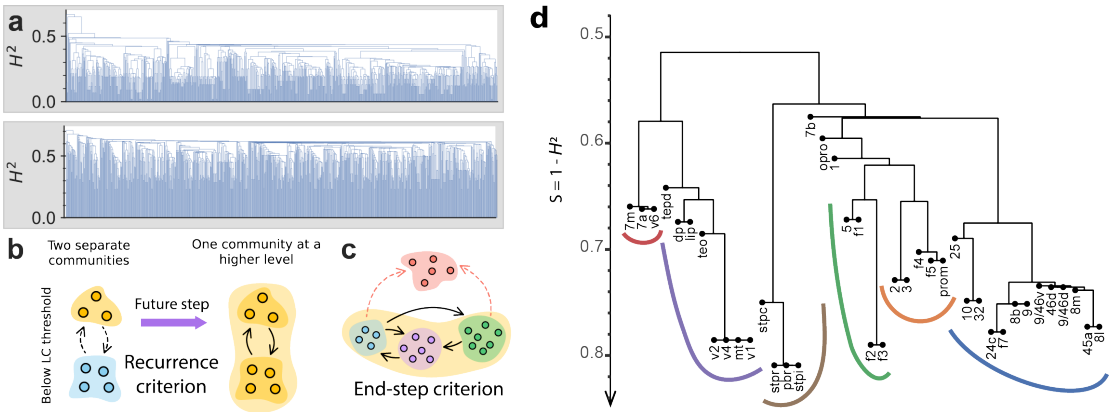

Fig. 3| Link- and node-community hierarchies in the macaque brain. a, The link-community hierarchy shown as a dendrogram for the data (top) and configuration model (bottom). The vertical lines at the lowest level represent individual links (999 links). Note that in the former it is more straightforward to appreciate the link-modular structure than in the latter. **b**, Node-community merging criterion based on reciprocal connectivity. **c**, Criterion for including into the hierarchy those node communities that were not included by the previous merging criterion. **d**, The resulting node-community hierarchy. The y-axis is the link-community similarity between node communities at their merging point, increasing from top to bottom. Areas that merged towards the bottom (for example V1 and V2) have more similar in- and out-neighborhoods than the ones that merged close to the top (7b, OPRO, etc.). We note that areas with strong topographic organization tend to merge towards the bottom of the hierarchy (V1, V2, MT, 3, 2, etc.). The colored arcs correspond to functional brain regions associated with object recognition (purple), movement detection (red), hearing (brown), motor (green), somatomotor (orange), and high-level cognitive functions (blue). The hierarchy's areal horizontal arrangement is computed by a software (ggtree) (Yu et al., 2017) and do not intent to display a special order.

Next, we increase th until it reaches the smallest value among all the link-community distances at that step, i.e., until $th = min_{i,j}\{d(C_i C_j)\}$. We then merge all pairs of communities separated by this distance value th into a new community at the next level, and we update the community list. This process is repeated until there is only one community left, see the **Extended Data Fig. 1**.

Fig. 3a shows the link-community hierarchy obtained with this method for the edge-complete component of the macaque dataset. It has many intricate structures, at all levels, indicating the complexity of the functional hierarchy. This also underscores our earlier statement that the link-community hierarchy has richer information than at the level of nodes. However, it is difficult to interpret the figure, because it shows essentially the ``cabling structure between the elements of a device'', not the elements and groups of elements of the device which are working together (considered to be the natural description of the inner workings of a system). We can, however, make a comparison of the link-community hierarchy in **Fig. 3**a (top), with the same generated from a null model, called the configurational model. The configuration model is a network obtained from the original network by randomly rewiring its connections (while maintaining edge weights). The link-community hierarchy for the configuration model (typical instance) is shown in **Fig. 3**a (bottom), showing that the link-community hierarchy for the original data is much more structured, indicating higher specificity and heterogeneity in its link-community structure.

Extracting the node-community hierarchy from the link-community hierarchy

As the link-community hierarchy is difficult to interpret, we need to generate a nodal community hierarchy using the link-community structure. This is possible because the link-community hierarchy also induces a partition on the nodal level. The main criterion that we use for generating the node communities is simple: at a given level two communities of nodes are merged if they are bidirectionally connected with edges from the same link community. We call this the “recurrence criterion”, i.e., the two groups must have recurrent connectivity within the same community of links (**Fig. 3**b). However, there are node groups that cannot be connected by this criterion, because, for example, they have only in-going, or out-going connections with the rest of the network (**Fig. 3**c); in these cases they are added into the node-community hierarchy at the end sequentially, in increasing order of their index. **Fig. 3**d shows the resulting node-community hierarchy, with the height of the branch between two newly merged groups being proportional to the difference in the H^2 distance between the link-communities at the merging event. The thick colored arcs correspond to functional regions in the cortex. The height difference between groups r on this dendrogram (see Glossary of terms) corresponds to the dissimilarity change between their weighted connectivity profiles.

To illustrate the relationship between the link and node level community hierarchies we consider the university structure in terms of interactions between professors at a university. At the smallest research group level, the professors (nodes) are “performing research in the field of physics and subfield of condensed matter”. In another group, other professors are “performing research in the field of physics and subfield of particle physics,” etc. In the chemistry department, a similar structure holds, with different research groups. Within each group there are numerus back-and-forth interactions (high local link density). There are fewer interactions between the research groups, and those are typically at faculty meetings where decisions are made affecting all groups. In this case, from the point of view of the department chair, these are groups “performing research in physics,” only – on a higher level of the functional hierarchy. The nature of discussions during faculty meetings will be specific to physics-based research needs. In the chemistry department, the same process happens and at their faculty meetings the discussions (interactions, functional links) will be specific to chemistry-based research needs. The two types of discussions in the two departments will clearly be different, although they will have commonalities. The two departments form two different nodal communities. The next level is at the College of Science, which houses both departments (and others). The dean is a mediator between these departments and when the dean has

a meeting of the chairs (each representing their departments), the discussions are at the level of departmental research needs and the potential return on those research activities (and less on research group specifics within the departments). When an issue arises that is beyond a particular research area (such as research space availability, graduate student stipends, etc.) then these functional activities (links) are running between all the departments, because decisions here globally impact the College of Science. At the next level, that of the provost, similar interactions occur, but now between the deans of the different colleges (Science, Arts and Letters, Engineering, etc.) through links that affect all at that level. If there was only links going in one direction between two groups than those groups do not belong to the same level of the hierarchy, one is subordinate to the other.

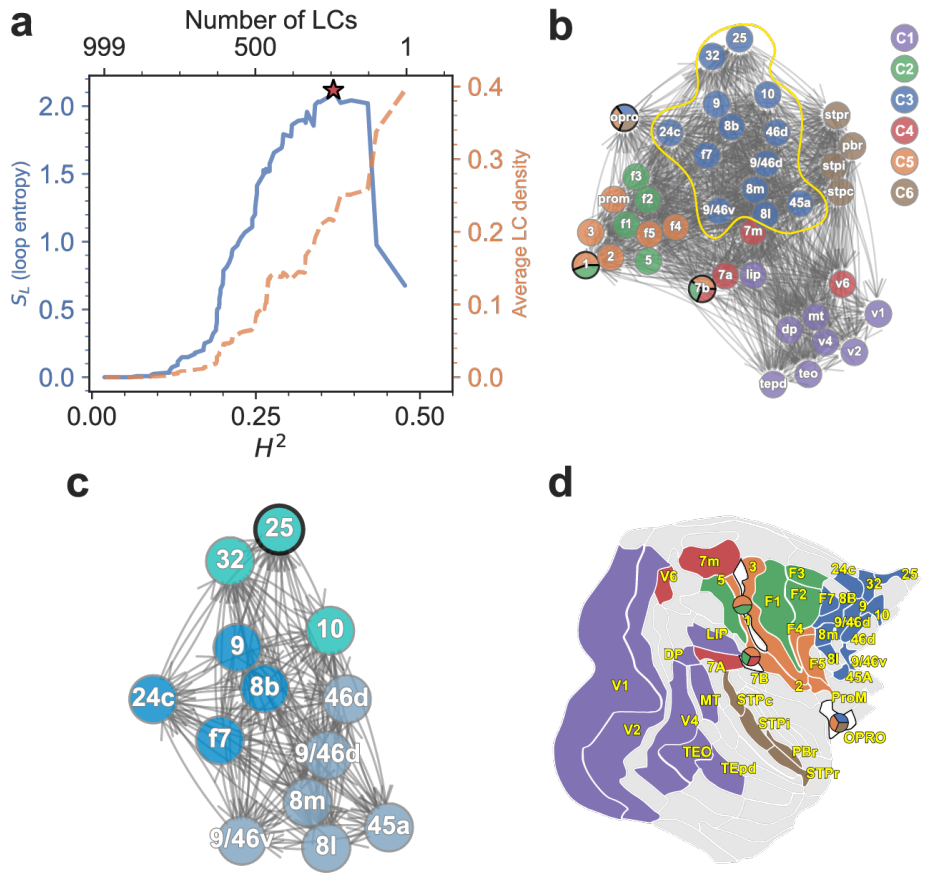

Fig. 4 | Community structure at an optimal level of the NC hierarchy. **a**, Distribution of the loop entropy S_L (solid line) and the average LC density (Ahn, Bagrow and Lehmann, 2010) (dashed line) as function of dissimilarity H^2. **b**, The optimal node-community structure corresponding to the maximum loop entropy value (the star in **a**). Nodes with pie-charts in them represent nodes with overlapping communities (NOCs; see **Table 1** for more information about them). **c**, The sub-community structure (a few levels below) of the blue community from **b** within the yellow loop. Area 25 community membership was found later using the cover assignment algorithm (see Methods section for more information). **d**, The optimal NC structure on the cortical flat map. Grey areas do not belong to the 40x40 edge-complete graph.

An optimal level of the node-community hierarchy

The node-community hierarchy shows the network of clusters from the most detailed level (one node in every cluster) to the least (the whole network is one cluster). The first is too

detailed, effectively not seeing the forest for the trees, and the latter is structurally uninformative. While the hierarchy as a whole provides an overall picture of the network's structural organization, we might wonder if there is an “optimal,” or a most informative level in the hierarchy. (Ahn, Bagrow and Lehmann, 2010a) uses the average link density over all link communities to identify such a level (see Methods), which, in the sparse network examples used in that study, has a peak somewhere in the middle of the hierarchy. However, for dense networks such as in cortex, this does not work as link densities increase all the way to the top of the hierarchy (**Fig. 4**a). Here we have modified the density measure in such a way that it has a robust peak at a certain level within the hierarchy and it is always guaranteed to have such a peak. The process used is similar to the Ahn et al measure, by considering the number of links in excess of the tree structure within each link community, but instead of calculating a density, calculates an entropy measure and chooses the hierarchy level that maximizes this “loop entropy” (see Methods). The optimal level in the link-community hierarchy is thus the one in which the distribution of the “excess” links (i.e. links generating loops and thus recurrence of information flow) is the most uniformly distributed across all link communities. The level defined in this manner is the most homogeneous from the point of view of recurrence. It is easy to show that at either end of the link-community hierarchy $S_L = 0$ and thus it must always exhibit a single global maximum. Given that the node-community hierarchy is derived from the link-community hierarchy, we simply use this correspondence to read off the level of the optimal node-community hierarchy. This shows

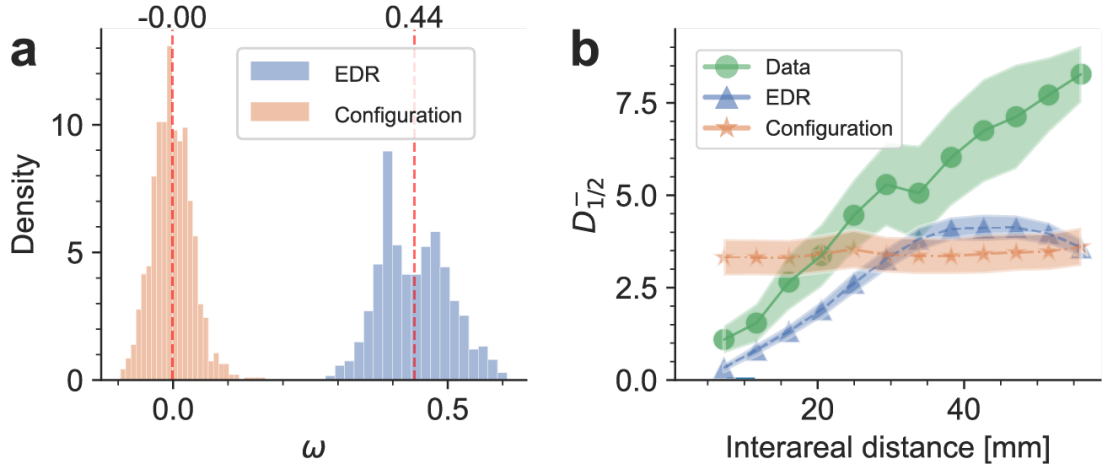

Fig. 5 | Comparison with models. **a**, Distribution of the omega index (a measure of the overall amount of overlap between two community structures; see Methods) for two network models, namely, the configuration model and the EDR model. The vertical dashed lines correspond to the average values after 1000 network samples. **b**, Similar plot as in **Fig. 2**b for $D^{-}_{1/2}$ of the data and the same for the two models. Lines and markers denote the average trends. Uncertainty band widths are equal to one standard deviation.

that at the optimal level, the macaque 40x40 dataset has a total of 6 communities (**Fig. 4**b,c). This will certainly change as the dataset grows, but the algorithm works the same way, identifying the optimal level in any version of the extended dataset. In the **Extended Data Fig. 2**, we show that the same analysis in the ECN with 29 (N. T. Markov *et al.*, 2014) injected areas results in similar node-community hierarchical structures.

Nodes with overlapping communities

The algorithm generates a small number of nodes that have multiple community memberships, i.e., nodes with overlapping communities, or NOCs (**Fig.** 4b). Such nodes are likely multifunctional, shown with a pie-chart structure in **Fig. 4**b. While this set will likely change with the growth of the dataset, some may likely be preserved. For a more detailed description of how areas are assigned to one or more communities see the Methods section.

Model comparison

In order to quantify how much overlap there is between the community structure of a model and that in the data, we use the notion of omega index (Gregory, 2011), see the Methods section. The value of $\omega = 1$ corresponds to perfect overlap between model and data. In **Fig. 5**a, we show the distribution of the omega index for two network models, namely the configuration model and the EDR model. The EDR model (Ercsey-Ravasz *et al.*, 2013) corresponds to a maximum entropy principle based generative interareal network model that uses the observed exponential decay of axonal bundle lengths with exponent λ (for the 40x91 dataset this is $\lambda = 0.16\, mm^{-1}$) and the same matrix of distances between the areas as in the dataset. In **Fig. 5**a, the red vertical dashed lines represent the averages of the omega index over 1000 network samples from the respective models. The fact that $\langle\omega\rangle = 0$ for the configuration model means that the connectivity randomization completely removes the community structure found in the dataset. In the EDR model $\langle\omega\rangle = 0.44$, showing that the EDR not only captures most of the summary statistics of the data (Ercsey-Ravasz *et al.*, 2013; Markov, Mária Ercsey-Ravasz, *et al.*, 2013), but also a good portion of its community structure. In **Fig. 5**b, we plot the $D^{-}_{1/2}$ divergence for all area pairs for the two models and the data, as a function of the distance between the pairs, showing that randomization indeed completely removes the heterogeneity of the structural organization in space for the configuration model, whereas the EDR captures fairly well the same trend, up to long distances. Note the plot for EDR at long distances is sensitive to the $\lambda = 0.16\, mm^{-1}$ value and additional injections might change that.

Relationship with the SLN-based hierarchy.

The fact that the interareal network of the macaque cortex is a hierarchically organized structure has been known since the seminal work of Felleman and van Essen (Felleman and Van Essen, 1991), which captured a version of this hierarchy exploiting the Feedforward/Feedback (FF/FB) nature of the visual pathways. This has later been better specified with the use of a quantitative measure (Barone *et al.*, 2000; Falchier *et al.*, 2002; Nikola T. Markov *et al.*, 2014; D'Souza *et al.*, 2022), called the fraction of labeled supra-granular layer neurons (SLN), obtained from tract-tracing experiments. Links with $SLN > 1/2$ are FF connections, with $SLN < 1/2$ are FB and with $SLN \cong 1/2$ lateral connections. We will refer to the hierarchy built with SLN as SLN-hierarchy (SLNh). In SLNh, FF compared to FB, *i)* crossed fewer levels of the hierarchy, *ii)* are topologically more organized, *iii)* are stronger and are *iv)* significantly fewer. SLNh ranks but does not define communities of nodes in the traditional network science sense.

Our node-community hierarchy (NCh) uses only connection strengths (in form of FLN values, but no SLN is used) and the connectivity matrix. It is also based on an entirely different criterion for defining the levels of the hierarchy, namely the Hellinger distance, as a measure of hierarchical depth or ranking. Moreover, our method focuses on finding network communities based on the recurrence of connections within a strength class, not on merely ranking the nodes. The fact that these communities also end up organized into a hierarchy of communities, is a direct outcome of the network structure. Finally, the NCh

is a description of the organization of the whole network (its edge-complete component). Despite these fundamental differences, however, there similar features in the two hierarchies and support common conclusions, as we describe below.

Since NCh does not use SLN values, the FF/FB nature of connections is not resolved. However, the Hellinger distance, which our algorithm uses to generate the NCh, and the absolute deviation of the SLN from ½ for all the links in the dataset, are correlated for both FF and FB connections (**Fig. 6**). This shows that on average there is a linear correlation between the depth/rankings of the two hierarchies, although with wide fluctuations (two-sided Pearson's correlation $r_{FF} = 0.43$ and $r_{FB} = 0.45$ with degrees-of-freedom, $dof_{FF} = 431$ and $dof_{FB} = 537$ for feedforward and feedback connections, respectively; $P < 10^{-5}$). The horizontal line at $H_{-}^{2} = 0.37$ corresponds to the optimal level in the NCh.

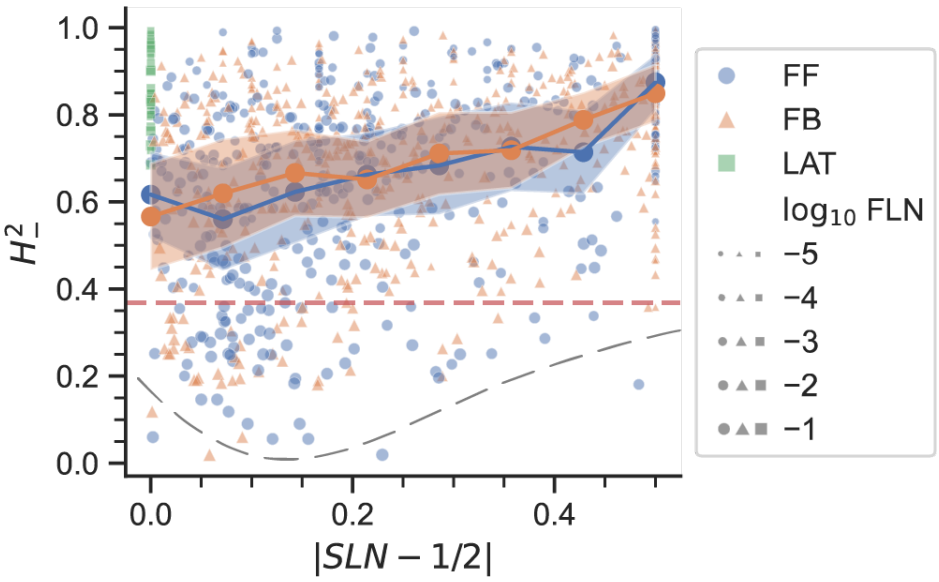

Fig. 6| Connection with SLN measures. The Hellinger distance between the endpoints of all the links as function of the deviation of their SLN values from ½. The size of the markers is proportional to the $log_{10} FLN$ values, i.e., the strength of the connections. Larger markers correspond to stronger connections. Blue markers denote feedforward (FF, $SLN > 0.5$) connections, whereas orange markers denote feedback (FB, $SLN < 0.5$) links. The green squares describe links corresponding to strongly lateral connections ($SLN \cong 0.5$). The red horizontal line is at $H_{-}^{2} = 0.37$ corresponding to the optimal level in the NCh. The dashed curvy line is guide to the eye signaling that links within the lower levels of the NCh up to the optimal level, have an SLN closer to 1/2., i.e., they are not strongly FF/FB and are also of large weight. Lines show H_{-}^{2} average trend. Uncertainty bands are the same as in **Fig. 5**b.

The gray dashed line is a guide to the eye showing that most links at the lower levels of the hierarchy (up to the optimal one) are more balanced, that is, they are not strongly FF/FB and that they have large weight (strong links). Interestingly, while there are overall 24% more FB links than FF in the whole edge-complete dataset, under the red straight dashed line (that is within the lower levels of the NCh), the roles are reversed: there are 31% more FF connections than FB. Furthermore, the FB connections are more scattered distribution across the Hellinger hierarchy scale than the FF connections, which are more organized. Thus, the Hellinger distance-based hierarchy generates similar observations to *i-iv)* above.

Discussion

In this paper we presented a principled approach to extracting the community structure of the macaque interareal cortical network and its hierarchical organization. Given a similarity measure or a distance measure, a node community is defined as a set of nodes that are similar/closer to each other by this measure than to the rest of the network. The bigger the difference between the intra-community distances and the distances to the outside of the community, the sharper is the identity of that community. A community detection algorithm's role is then to identity these subgraph structures. Changing the scale of resolution, the communities may form communities themselves, thereby giving rise to a hierarchical organization of the communities across several scales. Accordingly, the whole network is described by this hierarchical structure, with single-node communities at the lowest level and the whole network forming a single community at the topmost level. Note, the same concepts can be applied to other structural elements of a network, such as links/edges. In this case, we need a similarity or distance measure between links; now communities are formed by groups of links closer to one-another than to the rest of the links in the network. These are called link-communities and the corresponding hierarchy the link-community hierarchy (LCh). Since in connected networks there are typically more links than nodes (trees being the only exception), link communities provide more detailed information than the node communities but are also harder to interpret. As the interareal network of the mammalian cortex is extremely dense, directed and weighted, many standard community detection methods perform poorly or fail altogether. This is mostly because the similarity measure used in such studies is related to local connection density, which is not a well-contrasting feature in networks that are in themselves globally dense.

Here we introduced a novel approach to community detection, applicable to such networks, and employs measures and criteria that are based on notions directly related to the functionality of these networks, as information processing structures. Our approach embeds the nodes of the network into a metric space, allowing for consistent comparisons and a well-defined hierarchical depth scale. To do that, we exploited the fact that the link weights (which are axonal bundle strengths) can be interpreted as probabilities and thus allowing the use of the Hellinger metric (frequently used in statistics and information theory) to generate the distances between nodes in this space. Note, our approach can be used in any network in which link weights are probabilities or can be interpreted as such. The link weights in our case are the fraction of labeled neurons (FLNs) obtained from retrograde tract-tracing experiments and are proxies for communication bandwidth between the functional areas (Markov, Mária Ercsey-Ravasz, *et al.*, 2013). The set of connection/communication strengths (or probabilities) between a node and the rest of the network forms its connectivity profile. Accordingly, the Hellinger distance between two nodes is a measure of dis-similarity between their connection profiles. Note that the Hellinger metric is well-defined even for two nodes that are not connected. Its relationship to one of the entropy rates, namely the ½-Rényi divergence, has an interpretation as an error exponent, used in hypothesis testing in the statistical literature. Here it serves as a measure for the statistical distinguishability of areal neighborhoods and interestingly, has a linear scaling with the physical separation of the areas. This further corroborates previous observations that connection profiles diverge with spatial separation, on average (Markov, Maria Ercsey-Ravasz, *et al.*, 2013). Our contribution here is to express this with an information theoretic measure. Moreover, it has a practical interpretation as a sample complexity, i.e., as the number of samples we need to draw (either structurally, as performed in tract-tracing experiments or dynamically) from one of the distributions in order to tell it apart from the other one (the ground truth distribution). Finally, the other interesting feature we found was that the ½-Rényi divergence is distributed according to

a Weibull distribution, from extreme value statistics (goodness of fit to the Weibull has an AIC index of 3554.0, whereas for the Gamma and the Lognormal distributions are 3569.4 and 3590.0, respectively). It is to be noted that the same distribution was found to describe shortest path distributions in random networks (Bauckhage, Kersting, Rastergahpanah, 2013), a possible connection to our case here.

Note, one might consider as an alternative to the Hellinger measure the physical distance between the areas. This is because functional dissimilarity increases, on average, with physical separation between the areas, and one might expect that this would generate similar results. The fact that this does not work well, is demonstrated in the Methods section.

Function in the brain is associated with links between areas that process information. When extracting the link communities (Ahn, Bagrow and Lehmann, 2010a), the sequential link merging process first merges those links that perform very similar functions, and then gradually those link communities that are increasingly different (but can be merged at that level). At this stage the loop entropy S_L (**Fig. 4**a) starts to increase, meaning that recurrence between the nodes of the link community also increases and the information flow structures become more complex, possibly playing the role of information integration across various computational modalities. Recurrence, or bidirectional information flow allows fast and reciprocal coordination between different functional modalities, for example to generate a fast motility response to a stimulus involving both visual and auditory streams. This is why, when creating the node communities from the LCh we chose a merging criterion that demands recurrence between two node communities with links that belong to a given functional modality (i.e., to a given link community at that level). Regarding the selection of the optimal level of the NCh, we choose that in which recurrence has the most uniform distribution, assuming that it is a good representative of the operational community structure. To observe the importance of having a meaningful community partition, see the **Extended Data Fig. 3**, where we show the matrix representation of the ECN with a random ordering and by using the arrangement obtained from the NCh. For the macaque the optimal community hierarchy level is at $H^2 \cong 0.37$, corresponding to 57 link communities and 98% of the links (981/999) belonging to non-tree communities. The associated node-community network at this level has 6 communities. In lieu of validation, when we applied our algorithm to benchmark networks (sparse) with predefined community structures in it, correctly identifying those communities (see **Extended Data Fig. 4**).

The resulting NCh shown in the dendrogram in **Fig. 3**d, has some interesting properties. First, the most similar areas are at the lower levels. The thick colored arcs represent branches in the hierarchy as generated by the algorithm, that agree with known functional systems in the brain. Note, this is generated by our algorithm, not "put in by hand". For example, the branches above the purple arc correspond to the ventral or "what" pathways, while those above the red arc to the "where" pathways. The others have similar interpretations from the auditory, somatosensory, premotor, motor and even prefrontal regions. This is remarkable, because the standard hierarchical view of processing places the primary (e.g., visual) areas as lowest level of the hierarchy, and the rest above. Our findings suggest that even those high-level areas that are not clearly associated with senses – they likely have other complicated connections with other subcortical structures – form their own pathways (sub-hierarchies), linked to attention, decision making or emotions. Our algorithms allow to disentangle in a principled way across the whole network, the heterogeneous and granular nature of functional processing in the brain.

Another interesting observation is that the low-level areas in **Fig. 3**d, are areas with strong topographic properties (V1, V6, 3, 2), i.e., with highly organized inputs. In these areas local changes in stimulus correspond to spatially local changes in the neurons

activated. This is plausible, since the brain needs to select very specific information incoming from the external world to generate the correct responses (for example, for survival). The neighbors of these areas are also topographic (**Fig. 3**d).

Our algorithm identifies nodes with overlapping communities, i.e., they do not have a strong membership in any of the communities but belong to two or more. These NOCs, we believe play a crucial role in coordinating information flow between multiple systems.

Comparisons of our NCh with that obtained in other models, show that randomization eliminates the hierarchical organization, and thus the structures found by our algorithms signal a strong and very specific functional organization in the cortex. The EDR model, based solely on the exponential decay of connectivity with distance and the matrix of distances, however, captures about 44% of the organization (according to the omega index), which means that the rest is due to other, possibly more biological factors, that remain to be elucidated.

The SLNh tracks information flow forward and back through the links categorized by their SLN value into FF and FB. The SLN is additional information, independent from the link weights (FLN) and it is strictly a two-point descriptor. While the FLN is also associated to two points, its value is relative to the other link strengths in the target node's network neighborhood (through the normalization factor). Note, the fraction of labeled supra-granular neurons can be either very low or very high depending on whether in a given source area we have relatively large number of labeled neurons. It was found (Markov et al, 2014) that a hierarchical level scale can be extracted from the SLN values using a beta-binomial model with adjustable dispersion parameter, which then was used to construct the SLN-hierarchy. There are two crucial differences between the SLNh and NCh. For one, the hierarchical level scale, the Hellinger distance, is solely based on connection strengths (so less informative) but it provides a principled and natural metric without any adjustable parameters trying to fit to a hierarchy. Second, the SLNh places individual nodes on the levels of the hierarchy, whereas the NCh places activity-specific communities. The subordination relationship in the NCh is a subset (inclusion) relationship: a community at a given level is formed by a grouping of smaller communities at a lower level. This is very different from the SLNh, which does not identify communities and their organization across scales. However, since both representations refer to the same information processing network, there must be some connection between the two. Indeed, this was illustrated in **Fig. 6**: when plotting the Hellinger distance between a connected pair of areas as function of their degree of FF/FB-character, a linear correlation has been found, showing that on average, the two hierarchical scales are correlated. Moreover, we discovered that connected node pairs, whose Hellinger distance is below the optimal community hierarchy threshold are 31% more FF than FB, and since they are the building blocks of the whole hierarchy, it means that the network at a backbone level is more of a driving (FF) structure than modulatory (FB), despite the fact that there are 24% more FB than FF in the whole network. We believe that the two types of hierarchies complement each other and when taken together, they offer a more holistic interpretation of information processing in the brain.

References

Ahn, Y.-Y., Bagrow, J.P. and Lehmann, S. (2010a) 'Link communities reveal multiscale complexity in networks', *Nature*, 466(7307), pp. 761–764. Available at: https://doi.org/10.1038/nature09182.

Ahn, Y.-Y., Jeong, H. and Kim, B.J. (2006) ‘Wiring cost in the organization of a biological neuronal network’, *Physica A: Statistical Mechanics and its Applications*, 367, pp. 531–537. Available at: https://doi.org/10.1016/j.physa.2005.12.013.

Barone, P. *et al.* (2000) ‘Laminar Distribution of Neurons in Extrastriate Areas Projecting to Visual Areas V1 and V4 Correlates with the Hierarchical Rank and Indicates the Operation of a Distance Rule’, *Journal of Neuroscience*, 20(9), pp. 3263–3281. Available at: https://doi.org/10.1523/JNEUROSCI.20-09-03263.2000.

Bassett, D.S. and Sporns, O. (2017) ‘Network neuroscience’, *Nature neuroscience*, 20(3), pp. 353–364. Available at: https://doi.org/10.1038/nn.4502.

Bastos, A.M. *et al.* (2012) ‘Canonical Microcircuits for Predictive Coding’, *Neuron*, 76(4), pp. 695–711. Available at: https://doi.org/10.1016/j.neuron.2012.10.038.

Batardiere, A. *et al.* (1998) ‘Area-specific laminar distribution of cortical feedback neurons projecting to cat area 17: Quantitative analysis in the adult and during ontogeny’, *Journal of Comparative Neurology*, 396(4), pp. 493–510. Available at: https://doi.org/10.1002/(SICI)1096-9861(19980713)396:4<493::AID-CNE6>3.0.CO;2-X.

Bhattacharyya, A. (1946) ‘On a Measure of Divergence between Two Multinomial Populations’, *Sankhyā: The Indian Journal of Statistics (1933-1960)*, 7(4), pp. 401–406.

Bodlaj, J. and Batagelj, V. (2015) ‘Hierarchical link clustering algorithm in networks’, *Physical Review E*, 91(6), p. 062814. Available at: https://doi.org/10.1103/PhysRevE.91.062814.

Bullmore, E. and Sporns, O. (2009) ‘Complex brain networks: graph theoretical analysis of structural and functional systems’, *Nature Reviews. Neuroscience*, 10(3), pp. 186–198. Available at: https://doi.org/10.1038/nrn2575.

Buzsáki, G. (2010) ‘Neural Syntax: Cell Assemblies, Synapsembles, and Readers’, *Neuron*, 68(3), pp. 362–385. Available at: https://doi.org/10.1016/j.neuron.2010.09.023.

Cam, L.L. and Yang, G.L. (2000) *Asymptotics in Statistics: Some Basic Concepts*. 2nd edition. New York Berlin Heidelberg: Springer.

Canonne, C.L. *et al.* (2019) ‘The structure of optimal private tests for simple hypotheses’, in *Proceedings of the 51st Annual ACM SIGACT Symposium on Theory of Computing*. New York, NY, USA: Association for Computing Machinery (STOC 2019), pp. 310–321. Available at: https://doi.org/10.1145/3313276.3316336.

Clauset, A., Moore, C. and Newman, M.E.J. (2008) ‘Hierarchical structure and the prediction of missing links in networks’, *Nature*, 453(7191), pp. 98–101. Available at: https://doi.org/10.1038/nature06830.

Cormen, T.H. (ed.) (2007) *Introduction to algorithms*. 2nd. ed., 10th pr. Cambridge, Mass.: MIT Press [u.a.].

Csiszar, I. (1995) ‘Generalized cutoff rates and Renyi’s information measures’, *IEEE Transactions on Information Theory*, 41(1), pp. 26–34. Available at: https://doi.org/10.1109/18.370121.

D’Souza, R.D. *et al.* (2022) ‘Hierarchical and nonhierarchical features of the mouse visual cortical network’, *Nature Communications*, 13(1), p. 503. Available at: https://doi.org/10.1038/s41467-022-28035-y.

Ercsey-Ravasz, M. *et al.* (2013) ‘A Predictive Network Model of Cerebral Cortical Connectivity Based on a Distance Rule’, *Neuron*, 80(1), pp. 184–197. Available at: https://doi.org/10.1016/j.neuron.2013.07.036.

van Erven, T. and Harremos, P. (2014) ‘Rényi Divergence and Kullback-Leibler Divergence’, *IEEE Transactions on Information Theory*, 60(7), pp. 3797–3820. Available at: https://doi.org/10.1109/TIT.2014.2320500.

Falchier, A. *et al.* (2002) ‘Anatomical Evidence of Multimodal Integration in Primate Striate Cortex’, *Journal of Neuroscience*, 22(13), pp. 5749–5759. Available at: https://doi.org/10.1523/JNEUROSCI.22-13-05749.2002.

Felleman, D.J. and Van Essen, D.C. (1991) ‘Distributed hierarchical processing in the primate cerebral cortex’, *Cerebral Cortex (New York, N.Y.: 1991)*, 1(1), pp. 1–47. Available at: https://doi.org/10.1093/cercor/1.1.1-a.

Fortunato, S. (2010) ‘Community detection in graphs’, *Physics Reports*, 486(3), pp. 75–174. Available at: https://doi.org/10.1016/j.physrep.2009.11.002.

Froudist-Walsh, S. *et al.* (2021) ‘A dopamine gradient controls access to distributed working memory in the large-scale monkey cortex’, *Neuron*, 109(21), pp. 3500-3520.e13. Available at: https://doi.org/10.1016/j.neuron.2021.08.024.

Gămănuţ, R. *et al.* (2018) ‘The Mouse Cortical Connectome, Characterized by an Ultra-Dense Cortical Graph, Maintains Specificity by Distinct Connectivity Profiles’, *Neuron*, 97(3), pp. 698-715.e10. Available at: https://doi.org/10.1016/j.neuron.2017.12.037.

Gregory, S. (2011) ‘Fuzzy overlapping communities in networks’, *Journal of Statistical Mechanics: Theory and Experiment*, 2011(02), p. P02017. Available at: https://doi.org/10.1088/1742-5468/2011/02/P02017.

Harris, J.A. *et al.* (2019) ‘Hierarchical organization of cortical and thalamic connectivity’, *Nature*, 575(7781), pp. 195–202. Available at: https://doi.org/10.1038/s41586-019-1716-z.

He, Y. and Evans, A. (2010) ‘Graph theoretical modeling of brain connectivity’, *Current Opinion in Neurology*, 23(4), pp. 341–350. Available at: https://doi.org/10.1097/WCO.0b013e32833aa567.

Hellinger, E. (1909) ‘Neue Begründung der Theorie quadratischer Formen von unendlichvielen Veränderlichen.’, *Journal für die reine und angewandte Mathematik*, 1909(136), pp. 210–271. Available at: https://doi.org/10.1515/crll.1909.136.210.

Henry, C.S. *et al.* (2016) 'Microbial Community Metabolic Modeling: A Community Data-Driven Network Reconstruction', *Journal of Cellular Physiology*, 231(11), pp. 2339–2345. Available at: https://doi.org/10.1002/jcp.25428.

Horvát, S. *et al.* (2016) 'Spatial Embedding and Wiring Cost Constrain the Functional Layout of the Cortical Network of Rodents and Primates', *PLOS Biology*. Edited by G. Konopka, 14(7), p. e1002512. Available at: https://doi.org/10.1371/journal.pbio.1002512.

HS Niederrhein - Dalitz (2020). Available at: https://lionel.kr.hs-niederrhein.de/~dalitz/data/hclust/#authors (Accessed: 28 July 2024).

Kamga, C., Krishnamurthy, S. and Shiva, S. (2012) 'Myoglobin and Mitochondria: A relationship bound by Oxygen and Nitric Oxide', *Nitric Oxide*, 26(4), pp. 251–258. Available at: https://doi.org/10.1016/j.niox.2012.03.005.

Lancichinetti, A. and Fortunato, S. (2009) 'Benchmarks for testing community detection algorithms on directed and weighted graphs with overlapping communities', *Physical Review E*, 80(1), p. 016118. Available at: https://doi.org/10.1103/PhysRevE.80.016118.

Li, K. and Pang, Y. (2013) 'Communities analysis in protein-protein interaction networks', in *2013 IEEE International Conference on Bioinformatics and Biomedicine*. *2013 IEEE International Conference on Bioinformatics and Biomedicine*, pp. 46–46. Available at: https://doi.org/10.1109/BIBM.2013.6732757.

Li, Y. and Turner, R.E. (2016) 'Rényi Divergence Variational Inference', in *Advances in Neural Information Processing Systems*. Curran Associates, Inc. Available at: https://papers.nips.cc/paper_files/paper/2016/hash/7750ca3559e5b8e1f44210283368fc16-Abstract.html (Accessed: 31 July 2024).

Mansour, Y., Mohri, M. and Rostamizadeh, A. (2009) 'Multiple source adaptation and the Rényi divergence', in *Proceedings of the Twenty-Fifth Conference on Uncertainty in Artificial Intelligence*. Arlington, Virginia, USA: AUAI Press (UAI '09), pp. 367–374.

Markov, N.T. *et al.* (2011) 'Weight Consistency Specifies Regularities of Macaque Cortical Networks', *Cerebral Cortex*, 21(6), pp. 1254–1272. Available at: https://doi.org/10.1093/cercor/bhq201.

Markov, N.T., Ercsey-Ravasz, Mária, *et al.* (2013) 'Cortical high-density counterstream architectures', *Science (New York, N.Y.)*, 342(6158), p. 1238406. Available at: https://doi.org/10.1126/science.1238406.

Markov, N.T., Ercsey-Ravasz, Maria, *et al.* (2013) 'The role of long-range connections on the specificity of the macaque interareal cortical network', *Proceedings of the National Academy of Sciences*, 110(13), pp. 5187–5192. Available at: https://doi.org/10.1073/pnas.1218972110.

Markov, N. T. *et al.* (2014) 'A Weighted and Directed Interareal Connectivity Matrix for Macaque Cerebral Cortex', *Cerebral Cortex*, 24(1), pp. 17–36. Available at: https://doi.org/10.1093/cercor/bhs270.

Markov, Nikola T. *et al.* (2014) 'Anatomy of hierarchy: Feedforward and feedback pathways in macaque visual cortex', *Journal of Comparative Neurology*, 522(1), pp. 225–259. Available at: https://doi.org/10.1002/cne.23458.

Mesulam, M.-M. (1990) 'Large-scale neurocognitive networks and distributed processing for attention, language, and memory', *Annals of Neurology*, 28(5), pp. 597–613. Available at: https://doi.org/10.1002/ana.410280502.

Meunier, D., Lambiotte, R. and Bullmore, E.T. (2010) 'Modular and Hierarchically Modular Organization of Brain Networks', *Frontiers in Neuroscience*, 4, p. 200. Available at: https://doi.org/10.3389/fnins.2010.00200.

Michalareas, G. *et al.* (2016) 'Alpha-Beta and Gamma Rhythms Subserve Feedback and Feedforward Influences among Human Visual Cortical Areas', *Neuron*, 89(2), pp. 384–397. Available at: https://doi.org/10.1016/j.neuron.2015.12.018.

Montgomery, D.C. (2020) *Introduction to statistical quality control*. Eighth edition, EMEA edition. Hoboken, NJ: Wiley.

Morales, D., Pardo, L. and Vajda, I. (2000) 'Rényi Statistics in Directed Families of Exponential Experiments*', *Statistics*, 34(2), pp. 151–174. Available at: https://doi.org/10.1080/02331880008802324.

Müllner, D. (2013) 'fastcluster: Fast Hierarchical, Agglomerative Clustering Routines for R and Python', *Journal of Statistical Software*, 53, pp. 1–18. Available at: https://doi.org/10.18637/jss.v053.i09.

Murray, G., Carenini, G. and Ng, R. (2012) 'Using the omega index for evaluating abstractive community detection', in *Proceedings of Workshop on Evaluation Metrics and System Comparison for Automatic Summarization*. USA: Association for Computational Linguistics (NAACL HLT '12), pp. 10–18.

Newman, M.E.J. (2004) 'Fast algorithm for detecting community structure in networks', *Physical Review E*, 69(6), p. 066133. Available at: https://doi.org/10.1103/PhysRevE.69.066133.

Newman, M.E.J. (2006) 'Modularity and community structure in networks', *Proceedings of the National Academy of Sciences*, 103(23), pp. 8577–8582. Available at: https://doi.org/10.1073/pnas.0601602103.

Nielsen, F. and Boltz, S. (2011) 'The Burbea-Rao and Bhattacharyya Centroids', *IEEE Transactions on Information Theory*, 57(8), pp. 5455–5466. Available at: https://doi.org/10.1109/TIT.2011.2159046.

Onnela, J.-P. *et al.* (2012) 'Taxonomies of networks from community structure', *Physical Review E*, 86(3), p. 036104. Available at: https://doi.org/10.1103/PhysRevE.86.036104.

Palla, G. *et al.* (2005) 'Uncovering the overlapping community structure of complex networks in nature and society', *Nature*, 435(7043), pp. 814–818. Available at: https://doi.org/10.1038/nature03607.

Pensia, A., Jog, V. and Loh, P.-L. (2024) ‘Communication-Constrained Hypothesis Testing: Optimality, Robustness, and Reverse Data Processing Inequalities’, *IEEE Transactions on Information Theory*, 70(1), pp. 389–414. Available at: https://doi.org/10.1109/TIT.2023.3334024.

Pensia, A., Loh, P.-L. and Jog, V. (2022) ‘Simple Binary Hypothesis Testing under Communication Constraints’, in *2022 IEEE International Symposium on Information Theory (ISIT)*. *2022 IEEE International Symposium on Information Theory (ISIT)*, pp. 3297–3302. Available at: https://doi.org/10.1109/ISIT50566.2022.9834363.

Pessoa, L. (2014) ‘Understanding brain networks and brain organization’, *Physics of life reviews*, 11(3), pp. 400–435. Available at: https://doi.org/10.1016/j.plrev.2014.03.005.

Rao, R.P.N. and Ballard, D.H. (1999) ‘Predictive coding in the visual cortex: a functional interpretation of some extra-classical receptive-field effects’, *Nature Neuroscience*, 2(1), pp. 79–87. Available at: https://doi.org/10.1038/4580.

Ravasz, E. *et al.* (2002) ‘Hierarchical Organization of Modularity in Metabolic Networks’, *Science*, 297(5586), pp. 1551–1555. Available at: https://doi.org/10.1126/science.1073374.

Ravasz, E. (2009) ‘Detecting Hierarchical Modularity in Biological Networks’, in R. Ireton et al. (eds) *Computational Systems Biology*. Totowa, NJ: Humana Press, pp. 145–160. Available at: https://doi.org/10.1007/978-1-59745-243-4_7.

Renyi, A. (1961) ‘On measures of entropy and information’, *1961* [Preprint].

de Reus, M.A. *et al.* (2014) ‘An edge-centric perspective on the human connectome: link communities in the brain’, *Philosophical Transactions of the Royal Society B: Biological Sciences*, 369(1653), p. 20130527. Available at: https://doi.org/10.1098/rstb.2013.0527.

Rosvall, M., Axelsson, D. and Bergstrom, C.T. (2009) ‘The map equation’, *The European Physical Journal Special Topics*, 178(1), pp. 13–23. Available at: https://doi.org/10.1140/epjst/e2010-01179-1.

Ruan, J., Dean, A.K. and Zhang, W. (2010) ‘A general co-expression network-based approach to gene expression analysis: comparison and applications’, *BMC Systems Biology*, 4(1), p. 8. Available at: https://doi.org/10.1186/1752-0509-4-8.

Saper, C.B., Scammell, T.E. and Lu, J. (2005) ‘Hypothalamic regulation of sleep and circadian rhythms’, *Nature*, 437(7063), pp. 1257–1263. Available at: https://doi.org/10.1038/nature04284.

Scheffé, H. (1956) ‘A “Mixed Model” for the Analysis of Variance’, *The Annals of Mathematical Statistics*, 27(1), pp. 23–36.

Shayevitz, O. (2011) ‘On Rényi measures and hypothesis testing’, in *2011 IEEE International Symposium on Information Theory Proceedings*. *2011 IEEE International Symposium on Information Theory Proceedings*, pp. 894–898. Available at: https://doi.org/10.1109/ISIT.2011.6034266.

Sporns, O. (2013) 'Structure and function of complex brain networks', *Dialogues in Clinical Neuroscience*, 15(3), pp. 247–262. Available at: https://doi.org/10.31887/DCNS.2013.15.3/osporns.

Sporns, O. and Betzel, R.F. (2016) 'Modular Brain Networks', *Annual Review of Psychology*, 67(Volume 67, 2016), pp. 613–640. Available at: https://doi.org/10.1146/annurev-psych-122414-033634.

Sporns, O., Tononi, G. and Kötter, R. (2005) 'The Human Connectome: A Structural Description of the Human Brain', *PLOS Computational Biology*, 1(4), p. e42. Available at: https://doi.org/10.1371/journal.pcbi.0010042.

Strong, D.R., Lawton, J.H. and Southwood, R. (1984) *Insects on plants: community patterns and mechanisms*. Cambridge, Mass: Harvard University Press.

Suresh, A.T. (2020) 'Robust hypothesis testing and distribution estimation in Hellinger distance'. arXiv. Available at: http://arxiv.org/abs/2011.01848 (Accessed: 20 February 2024).

Váša, F. and Mišić, B. (2022) 'Null models in network neuroscience', *Nature Reviews Neuroscience*, 23(8), pp. 493–504. Available at: https://doi.org/10.1038/s41583-022-00601-9.

Vezoli, J. *et al.* (2021) 'Cortical hierarchy, dual counterstream architecture and the importance of top-down generative networks', *NeuroImage*, 225, p. 117479. Available at: https://doi.org/10.1016/j.neuroimage.2020.117479.

Wu, K. *et al.* (2011) 'The Overlapping Community Structure of Structural Brain Network in Young Healthy Individuals', *PLOS ONE*, 6(5), p. e19608. Available at: https://doi.org/10.1371/journal.pone.0019608.

Yatracos, Y.G. (1985) 'Rates of Convergence of Minimum Distance Estimators and Kolmogorov's Entropy', *The Annals of Statistics*, 13(2), pp. 768–774. Available at: https://doi.org/10.1214/aos/1176349553.

Yu, G. *et al.* (2017) 'ggtree: an r package for visualization and annotation of phylogenetic trees with their covariates and other associated data', *Methods in Ecology and Evolution*, 8(1), pp. 28–36. Available at: https://doi.org/10.1111/2041-210X.12628.

Methods

Data

We rely on two datasets from retrograde tract-tracing experiments in the macaque monkey, obtained with consistent methods. The datasets are the matrices $G^{\mathrm{FLN}}_{91\times 40}$ and $G^{\mathrm{SLN}}_{91\times 40}$ of FLN and SLN values FLN_{ij} and SLN_{ij} for 40 injected target areas (i is a source area, projecting into target/injected area j), in a 91-area parcellation. The second one is the dataset that contains all pairwise distances along estimated shortest physical paths avoiding anatomical obstacles, between area barycenters, recorded in the matrix $D_{91\times 91}$. All data is available from (Froudist-Walsh *et al.*, 2021).

Community detection must be done in systems or subsystems with complete connectivity information. For that reason, from $G^{i}_{91\times 40}$ where $i \in \{\mathrm{FLN}, \mathrm{SLN}\}$, we extracted the subnetwork with 40 injected areas $G^{i}_{40\times 40}$ - also referred to as the edge-complete network (ECN) - whose connectivity and connection strength information have been measured between every pair of its nodes. Therefore, the communities and hierarchies are representative of the ECN, and that is not going to change when future injections are added to the dataset.

Probability mass functions of area connections

Let us define the set of areas from the whole network as U and from the ECN as $V \subseteq U$ with sizes $|U| = 91$ and $|V| = 40$, respectively. Each area $i \in V$ has two neighborhoods, one for its in- and another for its out-links. The in-neighborhood of (the target) area i is defined as

$$P_i^- \equiv \frac{\{FLN_{1i}, \ldots, FLN_{|U|i}\}}{\sum_{j=1}^{|U|} FLN_{ji}} = \{FLN_{1i}, \ldots, FLN_{|U|i}\}.$$

Note that this probability mass function has data from the 91 areas, with $P_i^-(j)$ representing the probability that a neuron is projecting from source area j into target area i, with normalization $\sum_{j=1}^{|U|} P_i^-(j) = 1$, due to the definition of the FLN.

For the out-neighborhoods, the probability mass functions will cover only areas in the ECN, because an injection reveals all the inputs from the rest of the network into the target area, but not the outputs. The outputs from a given source area need to be collected across all the injections. Since there are 40/91 injections, full connectivity information (and their FLN weights) exists only for the ECN. Thus, for (the source) area i, it is defined as

$$P_i^+ \equiv \frac{\{FLN_{i1}, \ldots, FLN_{i|V|}\}}{\sum_{j=1}^{|V|} FLN_{ij}}.$$

Thus, $P_i^+(j)$ represents the probability that a neuron sampled from source area i projects into target area j, given that it projects into some area of the ECN.

Hellinger distance

is a measure between two probability distributions (Hellinger, 1909; Cam and Yang, 2000). As explained in the main text, the Hellinger distance H is a metric, i.e., it satisfies the triangle inequality, and it is also bounded $0 \leq H \leq 1$. For simplicity, let us first define the squared-difference function $h(x, y) \equiv \left(\sqrt{x} - \sqrt{y}\right)^2$. In general, the squared Hellinger distance between the probability mass functions P and Q with common discrete support V is defined as:

$$H^2(P, Q) = \frac{1}{2}\sum_{i\in V} h(p(i), q(i)).$$

In our case the probability distributions are associated with the elements of the set of nodes V of the ECN, namely we are computing the squared Hellinger distance of the probability mass functions associated with nodes $A \in V$ (that is $P \equiv P_A$) and $B \in V$ ($Q \equiv P_B$) respectively, for all pairs of nodes (A, B). Thus, $p_A(i) \in P_A$ represents the probability that node $i \in V$ projects into (or from) node A. One can think of i's link to (from) A as an (projection) "event". The definition for $p_B(i) \in P_B$ is similar. Because the probability mass functions are associated to the elements of the support itself, the sum above needs to be

computed with care when $i = A$ or $i = B$, because in our dataset self-connections (intrinsic connections) are zero: $p_A(A) = p_B(B) = 0$. To illustrate that, assume that nodes A and B have identical neighborhoods (outside of A and B), and identical probability mass functions (including $p_A(B) = p_B(A)$). If we were to compute H^2 naïvely, element-wise, the terms $h(p_A(B), p_B(B))$ and $h(p_A(A), p_B(A))$ would both be non-zero, and we would obtain a non-zero squared Hellinger distance, $H^2(P_A, P_B) \neq 0$, which would be incorrect, given that the two distributions are identical. For this reason, the correct expression of the squared Hellinger distance that we need to use is:

$$H^2(P_A, P_B) = \frac{1}{2} \sum_{i \in V/\{A,B\}} h\big(p_A(i), p_B(i)\big) + \frac{1}{2} h\big(p_A(B), p_B(A)\big) \equiv \frac{1}{2} \sum\nolimits_{i \in V}' h\big(p_A(i), p_B(i)\big),$$

where we use a primed sum notation to indicate that the summation is to be taken as explained above. When applying the above in our calculations, we have to do that separately for the out-neighborhoods and the in-neighborhoods of the nodes, i.e., working with $H^2\big(P_A^{\pm}, P_B^{\pm}\big) \equiv H_{\pm}^2$.

Sample complexity

Is defined as the sufficient number of samples needed to correctly differentiate two distributions with a classification error rate $\delta \leq 0.1$ (see next), in a simple binary hypothesis test (Pensia, Loh and Jog, 2022). Suppose n samples are drawn from one of two probability distributions P and Q over support V. The test (function) ϕ: $\cup_{i=1}^{\infty} V^i \to \{P, Q\}$ that classifies samples $X = (x^1, \ldots, x^n) \in V^n$ to P or Q, solves the simple binary hypothesis test problem with sample complexity $\mathcal{N}^{\delta}(P, Q)$, if it is the smallest number that satisfies

$$\delta \geq \mathbb{P}_P[\phi(X) = Q] + \mathbb{P}_Q[\phi(X) = P],$$

where $\mathbb{P}_P[\phi(X) = Q]$ represents the (failure) probability of classifying the samples as coming from Q when drawn from P, and vice versa, for the second term (Pensia, Loh and Jog, 2022). Moreover, it is known (Canonne *et al.*, 2019) that it scales as

$$\mathcal{N}^{\delta}(P, Q) = \Theta\left(\frac{-\log \delta}{H^2(P, Q)}\right),$$

where $\Theta(\cdot)$ is the Big-Theta notation for asymptotic tight (upper and lower) bound (Cormen, 2007).

Finally, if ϕ is the optimal likelihood test and $n \gtrsim \frac{-\log \delta}{H^2(P,Q)}$ for $\delta \leq 0.1$, the failure probability of the test ϕ with n samples is less than δ (Pensia, Jog and Loh, 2024). In the case of the Scheffé's test $\mathbb{I}(x) = 1$ if $P(x) \geq Q(x)$ and 0 otherwise (Scheffé, 1956), it is at most $O\left(\frac{1}{H^4(P,Q)}\right)$ (Pensia, Loh and Jog, 2022; Pensia, Jog and Loh, 2024) for $\delta = 0.1$, where $O(\cdot)$ stands for the Big-O notation for the asymptotic upper bound (Cormen, 2007); but it has been found that it can be a tight bound for certain distributions (Suresh, 2020).

α-Rényi divergence

For two probability distributions P_A and P_B, the α-Rényi divergence (Renyi, 1961) is

$$D_\alpha(P_A||P_B) = \frac{1}{\alpha-1}\log\left(\sum_i' \frac{(p_{A(i)})^\alpha}{(p_{B(i)})^{\alpha-1}}\right),$$

where we already used the primed sum as defined for the Hellinger distance. This function has several properties. In particular, for any P and Q, $D_\alpha(P||Q)$ increases as a function of α. For $\alpha = 1$, $D_1(P||Q)$ is the Kullback-Leibler divergence, $D_{KL}(P||Q)$. For our purposes, the Rényi divergence of interest is the one with order parameter $\alpha = 1/2$, i.e.,

$$D_{1/2}(P_A||P_B) = -2\log\left(\sum_i' \sqrt{p_A(i)p_B(i)}\right).$$

We have chosen $\alpha = 1/2$ because it is the only Rényi divergence that is symmetric. This property is important since in our case, probability mass functions are associated with node neighborhoods. By comparing them, we do not aim to measure their information compression properties – a classical application of information divergence – but to measure how different they are. Moreover, since the probabilities of the same event from both probability mass functions, $p_A(i)$ and $p_B(i)$, are multiplied and not divided as in the Kullback-Leibler divergence (or any $\alpha \geq 1$), we can still measure their dissimilarity even if there are mutually exclusive events, i.e., events that have zero probability in one and non-zero in the other distribution. These two properties make the ½-Rényi divergence useful, since it makes it possible to relate network related quantities such as the similarity between node neighborhoods to information theory and statistical inference. Finally, it is associated with the squared Hellinger distance (Nielsen and Boltz, 2011) via equation (1). These functions allow us to decode the functional organization of the network from an information theoretic perspective (Shayevitz, 2011; Canonne *et al.*, 2019).

Similarity between directed links

The similarity of out-links e_{ij} and e_{ik} from common a node i is defined as $S(e_{ij}, e_{ik}) = 1 - H^2(P_j^-, P_k^-) = 1 - H_-^2$. For in-links e_{ji} and e_{ki}, the similarity measure is $S(e_{ji}, e_{ki}) = 1 - H^2(P_j^+, P_k^+) = 1 - H_+^2$. The reason for using the in-neighborhoods of nodes j and k when measuring the similarity between the out-links e_{ij} and e_{ik} from node i, is because e_{ij} and e_{ik} are in-links to nodes j and k, and in this way we are comparing in-links with in-links (one belonging to j, the other to k). In other words, the dissimilarity between directed links is the squared Hellinger distance of the uncommon nodes.

Link community algorithm example in a toy model

To explain how the link community algorithm works, we prepared a toy model using a simple directed binary network with three nodes and five links which is shown in the **Extended Data Fig. 1**a. First, each link is associated with a link community. Then, we create a complete graph whose nodes are network's links and whose link weights are the dissimilarities between them (**Extended Data Fig. 1**b). The algorithm starts by selecting a dissimilarity threshold th which is the lowest dissimilarity of the complete network (i.e., maximum similarity, $th = 0$). Then, link communities whose dissimilarities are equal to th are merged pairwise (link merging process), creating new link communities (**Extended Data Fig. 1**b-1)-3)). Next, the dissimilarity threshold is increased to the next minimum link community dissimilarity (in the example, th increases to $th = 0.29$), and the link merging process starts again (**Extended Data Fig. 1**b-4)). Note that as long as the dissimilarity between two members, one for each link community, equals to th, those link communities are merged. This is known as the single-linkage criterion (Müllner, 2013). The link merging

process and single-linkage criterion is repeated until there is only one link community left (**Extended Data Fig. 1**b-5)). The information as to which link communities merged and at which th, is then used to create a dendrogram, also referred as link-community hierarchy (**Extended Data Fig. 1**c).

Extracting the node-community hierarchy from the link-community hierarchy, using node merging criteria

As stated in the Results section, to derive the node-community hierarchy using the link community algorithm requires specifying how node communities merge through the link merging process. We use two criteria. i) The *recurrence criterion* where two node communities merge if they are connected by a link community with recurrent connections, i.e., links (from the same link community) directed both ways between the node communities; and ii) the *end-step criterion*, in which node communities that did not merge by the end of the link merging process are then merged pairwise and sequentially. An illustration of the node merging process can be seen in **Fig. 3**b-c. Note, the node-community hierarchy depends on these criteria. We choose the recurrence criterion because this is a key property in several multi-agent systems as it allows coordination of information/balance; an example is the mutual inhibition of the neurons in the ventrolateral preoptic and monoaminergic subcortical structures during sleep-wake transitions (Saper, Scammell and Lu, 2005). Moreover, it provides the advantage of stability (once two communities are merged, they will not split at any higher threshold value). Therefore, the node-community hierarchy is well-defined.

Loop entropy

We introduce here the notion of loop entropy, that will provide us with a criterion that allows us to select an "optimal" level in the link-community hierarchy. We start with the definition that trees (which are connected networks whose number of links M are related to its number of nodes N by the equation $M = N - 1$), have no (i.e., zero) community structure. To further simplify matters we will ignore the directionality of the links in what follows. We define the number of excess links M_{exc} of a network G with M links and N nodes as $M_{exc}(G) = M - N + 1$ (which is zero for a tree).

Suppose a network G is partitioned in L mutually exclusive subgraphs $g^L = \{g_i\}_{i=1}^L$ i.e., $G = \cup_{i=1}^L g_i$ and $\emptyset = g_i \cap g_j \; \forall i,j \in \{1, \dots, L\}$. Then, the loop entropy, S_L, of that partition is defined as

$$S_L(g^L) = -\sum_{i=1}^L p_{exc}(i) \log p_{exc}(i) - p_{tree}(g^L) \log p_{tree}(g^L),$$

where $p_{exc}(i) = \frac{M_{exc}(g_i)}{M_{exc}(G)}$ is the probability of sampling excess links in the subgraph g_i from the total number of excess links in G. Finally, $p_{tree}(g^L) = 1 - \sum_{i=1}^L p_{exc}(i)$ is a normalization factor.

The loop entropy is a measure of the distribution of excess links among the subnetworks, i.e., how much the partition differs from the tree (null) model which does not encode community information (recall, communities must have recurrent links). Since it is a Shannon-Gibbs type entropy, it is maximized when the distribution of excess links of the partition $P_{exc}(g^L) = \{p_{exc}(i)\}_{i=1}^L \cup p_{tree}(g^L)$ is uniform of the community structure.

Note, we have not proved that S_L can always be computed since it might occur that there are partitions where $M(g) > M_{exc}(G)$ for a particular subgraph g, or that $\sum_{i=1}^L M_{exc}(g_i) > M_{exc}(G)$ (in this case we no longer work with probabilities). However, we found that the score did not have such issues in the networks analyzed by us. Here we

use the loop entropy as a community quality score for link community partitions in various network models and benchmarks (Lancichinetti and Fortunato, 2009) and in all cases the S_L was well defined. Until there is a mathematical proof that S_L can be computed for any arbitrary mutually exclusive partition, we recommend monitoring the S_L values to find possible anomalies, when using it with the link community algorithm. See the **Extended Data Fig. 5** for an example.

Identifying the optimal node-community hierarchy level from the optimal link-community hierarchy

We can use the loop entropy to find an optimal LCh level. However, finding the correspondent NCh level is not straightforward. In the **Extended Data Fig. 6**, we explain our method with an example.

Cover assignment algorithm

At a selected level (other than the first) from the NCh, there might be single-node communities. However, it is still desired to assign them to one or several non-single node communities, i.e., with more than one member. In the **Extended Data Fig. 7** and its caption we explain how the algorithm works, with an illustration.

Omega index

It is a measure of the agreement between community partitions of a network when nodes can belong to more than one group or covers. To our best knowledge, it was published in reference (Gregory, 2011a). Assume there is a network with N nodes partitioned into two cover structures $C = \{C_i\}_{i=1}^{k}$ and $C' = \{C'_{i'}\}_{i'=1}^{k'}$ such that C_i ($C'_{i'}$) is the set of nodes in cover with index i (i') (not necessarily mutually exclusive). Then, their omega index is

$$\omega(C, C') = \frac{\omega_u(C,C') - \omega_e(C,C')}{1 - \omega_e(C,C')} ,$$

where

$$\omega_u(C, C') = \binom{N}{2}^{-2} \sum_{j=0}^{\max(k,k')} \left| t_j(C) \cap t_j(C') \right| ,$$

and

$$\omega_e(C, C') = \binom{N}{2}^{-2} \sum_{j=0}^{\max(k,k')} \left| t_j(C) \right| \left| t_j(C') \right| .$$

In the above equations, $t_j(\cdot)$ represents the set of node pairs that appear exactly j times in a cover. For example, suppose there are three nodes a, b, and c with two cover structures $C = \{(a,b,c),(c,d)\}$ and $C' = \{(a,b),(c,d),(a,d)\}$, with two and three covers, respectively. Then, $j \in \{0,1,2,3\}$. For $j = 0$, $t_0(C) = \{(a,d),(b,d)\}$ and $t_0(C') = \{(a,c),(b,d),(bc)\}$. So, $|t_0(C) \cap t_0(C')| = 1$, which means that only the pair (b,d) appears zero times in both cover structures. Note, that if a node pair belongs to t_0, it cannot belong to other t_j for any $j > 0$, i.e., $t_j(C)$ are disjoint sets (mutually exclusive).

Then, ω_u represents the probability of selecting randomly a node pair with equal frequency which is observed in both cover structures for some $t_j(\cdot)$; ω_e denotes the probability of sampling a node pair with equal frequency but which might not exist in both cover structures for some $t_j(\cdot)$. Finally, the term $1 - \omega_e$ is the normalization factor for the

case $\omega_u = 1$. Notice that $\omega = 1$ if and only if the node pair appearance frequency sets $t_j(\cdot)$ have the same elements for both cover structures and for all js, denoting a strong similarity/overlap.

Validation

To validate the performance of the algorithm, we generated weighted and directed Lancichinetti-Fortunato (LF) benchmarks with ground-truth node community memberships, allowing some nodes to participate in more than one cover (Lancichinetti and Fortunato, 2009) (see **Extended Data Fig. 4**). The benchmark generates networks with power-law degree and power-law community-size distributions. Here, we choose the degree and community size distribution exponents to be $t_1 = 2$ and $t_2 = 1$, respectively.

Additionally, the benchmark has topological mixing parameter μ_t and weight mixing parameter μ_w that control the complexity of the generated networks (explained next). Suppose k_i is the total degree of node i. Also, define the total strength of the node to be $s_i \equiv k_i^{\beta}$. Here, $\beta = 2$. Then, the internal degree $k_i^{(in)}$ and internal strength $s_i^{(in)}$ are the number of neighbors of node i and the sum of the weights of the links between node i and all the nodes of the network within the same cover as node i. They are defined as $k_i^{(in)} \equiv (1-\mu_t)k_i$ and $s_i^{(in)} \equiv (1-\mu_w)s_i$ with $\mu_t, \mu_w \in [0,1]$. By definition, the external degree $k_i^{(ext)}$ and external strength $s_i^{(ext)}$ are $k_i^{(ext)} = k_i - k_i^{(in)}$ and $s_i^{(ext)} = s_i - s_i^{(in)}$, respectively. Clearly, low values of μ_t or/and μ_w imply that most of the links or link strengths of a node are distributed within the communities belonging to the same cover as the node itself, signaling a sharp community structure. On the other hand, large values of μ_t or μ_w represent a more diffuse community structure.

Now, let w_{ij} denote the link weight of the link from node i to node j. The set of link weights $\{w_{ij}\}$ are generated randomly and then modified to minimize the function $\mathrm{Var}(\{w_{ij}\}) = \sum_i (s_i - \rho_i)^2 + \left(s_i^{(in)} - \rho_i^{(in)}\right)^2 + \left(s_i^{(ext)} - \rho_i^{(ext)}\right)^2$, where $\rho_i = \sum_j w_{ij}$, $\rho_i^{(in)} = \sum_j w_{ij}\kappa(i,j)$, $\rho_i^{(ext)} = \sum_j w_{ij}(1-\kappa(i,j))$, and $\kappa(i,j) = 1$ if nodes i and j have at least one common node-community membership, and 0 otherwise.

Here, μ_t was varied between 0.1 (compact communities; low complexity) to 0.8 (diffuse communities; high complexity) in steps of 7/90 (10 variations) while $\mu_w = 0.01$ is fixed. We choose a low μ_w because these networks are sparse, otherwise the external strength $s^{(ext)}$ would be distributed among only a small number of inter-community links, making them much stronger than the within-community links, a biologically non-plausible scenario.

Other parameters are the average and maximum degree $\langle k \rangle = \{5, 7, 10\}$ and $k_{\max} = \{30, 50\}$ (**Extended Data Fig. 4**); and the minimum and maximum community size parameters. Here they are 5 and 25, respectively.

We choose the generated benchmarks to have 100 nodes, where 5% of them participate in 2, 3 or 4 overlapping community memberships (Om), shown as columns in **Extended Data Fig. 4** and the rest of the nodes participate in only one. For each point in the parameter space, 100 instances were generated.

After generating the networks, we used our algorithm to find their cover structure, including multi-community memberships. We did that by computing the NCh of the networks and finding the optimal LCh level with the maximum average link community density $\langle D \rangle$ (Ahn, Bagrow and Lehmann, 2010) (as explained below) and loop entropy, S_L.

The average link-community density $\langle D \rangle$ on level l of the LCh in a network with M links is

$$\langle D \rangle_l = \sum_{c \in C(l)} D_c \frac{m_c}{M},$$

where $C(l)$ is the set of link communities at that level, D_c is the "effective" density of the link community $c \in C(l)$. We call it "effective" because it is the density relative to the link community tree null version (Ahn, Bagrow and Lehmann, 2010a), i.e.,

$$D_c = \frac{m_c - (n_c - 1)}{n_c(n_c - 1) - (n_c - 1)} = \frac{m_c - (n_c - 1)}{(n_c - 1)^2},$$

where m_c and n_c are the number of links and nodes of the link community $c \in C(l)$. As mentioned earlier, the number of links of the tree null version of a link community is $n_c - 1$, and the total possible number of links between the nodes of the link community is $n_c(n_c - 1)$ because the graph is directed in this case.

Once the optimal level is found in the LCh, we find the corresponding optimal level of the NCh. Then, we use the cover assignment algorithm to assign covers to possible single-community nodes and compute the omega index ω between the predicted and the ground-truth community structures. In the **Extended Data Fig. 4**, we show that S_L performs better on average than $\langle D \rangle$, in most of the cases, except the ones where communities are very dense such as the last row of **Extended Data Fig. 4**, where the large $\langle k \rangle = 10$ and the small $k_{\max} = 30$ results in compact node communities. In all other cases, S_L is a better score to identify the optimal node community partition.

Finally, we note that the weighted and directed networks with nodes that participate in multiple communities generated from the LF benchmark are very challenging for most state-of-the-art community detection algorithms; and none of those algorithms, as far as we know, work in dense networks. Unlike the algorithm presented here, they are not able to produce a NCh, encoding community information at multiple levels.

Using interareal distance as a dissimilarity measure

Here we briefly consider an alternative to the Hellinger distance (which ultimately is based on connectivity strengths), the physical interareal separation distance as "dissimilarity" measure. At first sight this seems acceptable, as according to the general observation areas that are more dissimilar (in function) are also further apart in space. Moreover, according to **Fig. 2**b, $D_{1/2}$ scales linearly, on average, with the interareal distance. However, also note that there is a significant amount of variation around the average, which likely holds valuable information, that the average does not capture. And this indeed is the case, as shown in **Extended Data Fig. 8** and described in its caption, in more detail.

Glossary of terms

Retrograde tract-tracing: It is an experimental procedure (Batardiere *et al.*, 1998; Barone *et al.*, 2000; Falchier *et al.*, 2002; Markov *et al.*, 2011) in which chemical markers injected into a region/area of the brain, called target, label the cell-bodies of the cells whose projections end in the injected area. The labeling happens through axonal transport from the terminal arbors to the soma of the cell. There is no secondary labeling.

Fraction of labeled neurons (FLN): Given a connection directed from node i to node j, its FLN value f_{ij} is the ratio between the number of neuronal labels found in source area i given an injection in target area j and the total number of labels extrinsic to j. It can be interpreted as the probability that neural activity in area i will induce (suppress) neural activity in area j (Falchier *et al.*, 2002; Markov *et al.*, 2011).

Edge-complete network (ECN): In this type of network, the connection and connection attributes, e.g., weight, between each network's node is known. Usually important when working with networks that are edge-incomplete, i.e., with missing connections.

EDR network model: The exponential distance rule (EDR) is the empirical observation (Ahn, Jeong and Kim, 2006; Ercsey-Ravasz *et al.*, 2013; Horvát *et al.*, 2016) that the distribution of the axonal lengths in the cortex decays exponentially, with a rate λ: $p(l) = ce^{-\lambda l}$, where l denotes the axonal (bundle) length, from the soma of the presynaptic neuron to the synapse with the postsynaptic neuron. The EDR network model is a generative interareal cortical random network model based on the maximum entropy principle that incorporates the EDR and the matrix of distances/lengths between the barycenters of the areas, see References (Ercsey-Ravasz *et al.*, 2013; Markov, Mária Ercsey-Ravasz, *et al.*, 2013; Horvát *et al.*, 2016; Gămănuţ *et al.*, 2018) for details on the model.

Dendrogram: Tree-like data structure that stores the relationships between datapoints.

Cover: It is a listing of the identities of all the node communities of a node. When the node belongs to just one community, its cover is formed by the id of that community; in case it belongs to multiple communities, its cover is the union of all identities.

Supragranular labeled neurons (SLN): Given a connection directed from node i to node j, its SLN value s_{ij} is the number of supra-granular neurons (above layer IV) divided by the total number across the cortical column found in source area i given an injection in target area j (Nikola T. Markov *et al.*, 2014). Its value is associated with two connection types with different physiological functions in the context of predictive coding. Values below 0.5 are called feedback (FB) and they typically propagate prediction probabilities from high- to low-level cortical areas; and above 0.5 are feedforward (FF) and typically propagate errors from the predictions made in low-level areas to high-level areas and have the role to update their internal state (Rao and Ballard, 1999; Barone *et al.*, 2000; Bastos *et al.*, 2012).

Software packages

We used Python 3.9.18 and libraries SciKit-Learn version 1.1.1, SciPy version 1.13.1, NetworkX version 2.8.8, and Pybind11 2.10.0. For plotting, we used Matplotlib version 3.5.2 and Seaborn version 0.13.2, and R-library ggtree version 3.8.2 (Yu *et al.*, 2017). Benchmarks were generated using the Lancichinetti-Fortunato model for directed, weighted, networks with nodes with multiple communities (Lancichinetti and Fortunato, 2009). We also used the hclust-cpp library that implements the hierarchical clustering algorithm (Müllner, 2013; *HS Niederrhein - Dalitz*, 2020). To compute the omega index, we used a publicly available code (Murray, Carenini and Ng, 2012).

Table 1. Cover neighborhood direction of the nodes with overlapping community membership in Fig. 4b. At the optimal loop entropy level, three areas do not merge with any non-single node community. As seen in **Fig. 4b**, the non-single node community ids are C1, C2, C3, C4, C5, and C6. Using the cover assignment algorithm, those areas are assigned to some non-single node communities by maximizing their average in/out-neighborhood similarity, or both (see Methods section). The neighborhood direction information is shown here.

Area	In	Out	Both

7b	C2 and C4	-	C5
1	C2	-	C5
OPRO	-	C3 and C6	C5

Data availability
The network connectivity data is available from https://core-nets.org/.

Code availability
The codes used in this study can be obtained via request to JMA.

Acknowledgments
This work was supported by the National Science Foundation (NSF) grant IIS-1724297 (J.M.A., Z.T.), French National Research Agency (ANR) grants A2P2MC ANR-17-NEUC-0004 (K.K., H.K.), ANR-17-FLAG-ERA-HBP-CORTICITY (to H.K. ANR-19-CE37–0025-DUAL_STREAMS (to K.K.).

Author contributions
The authors would like to express their thanks for discussions with B. Molnár, L. Magrou, Y. Hou. JMA and ZT designed the research, JMA wrote all the algorithms and ran the simulations, JMA performed the computational and data analysis with guidance from ZT, KK and HK provided the experimental datasets, JMA and ZT wrote the paper with assistance from KK and HK, and all authors contributed to editing the paper.

Competing interests
The authors declare no competing interests.

Additional information
Extended data are found below.

Correspondence and request for materials should be addressed to Z.T.

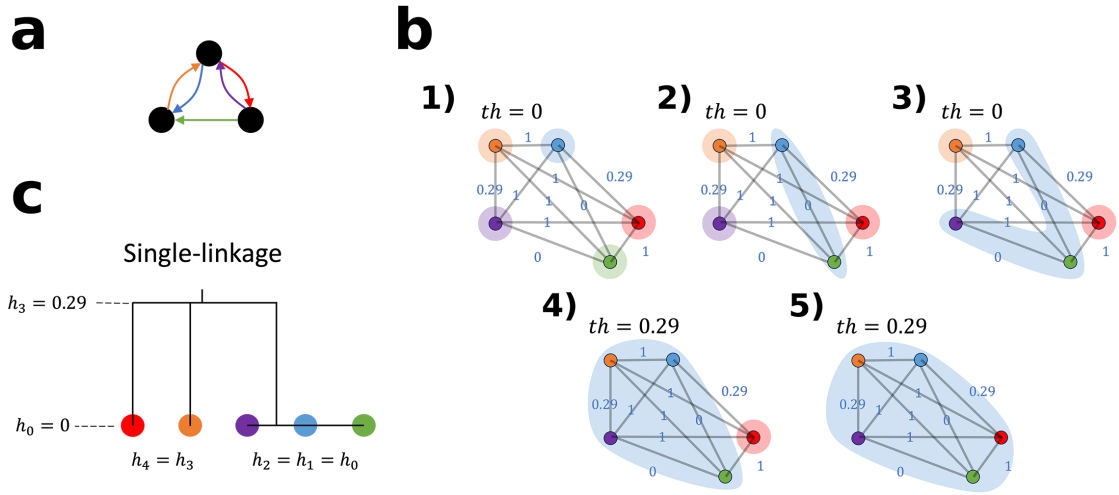

Extended Data Fig. 1| Link community algorithm example. a, To illustrate how the link community algorithm works, we use a toy binary directed network with three nodes and five links. Each link is color differently. In **b**, the network's nodes are associated with the links in **a**. The H^2 dissimilarity between links is written with a blue number. **b1)-b3),** The algorithm starts out by setting the lowest link dissimilarity threshold $th = 0$ then merging pairwise those links whose dissimilarity is equal to the threshold. **b4),** If no more link community pairs can be merged, the threshold is increased to the next lowest link dissimilarity value. Note that as soon as the dissimilarity between two members (one for each link community) equals to th, the link communities are merged. This rule is known as the single-linkage criterion. **b5),** The process of merging link community pairs and increasing the threshold continues until there is only one link community left. **c,** The information about which link community pairs merged at which th value is stored in the LCh.

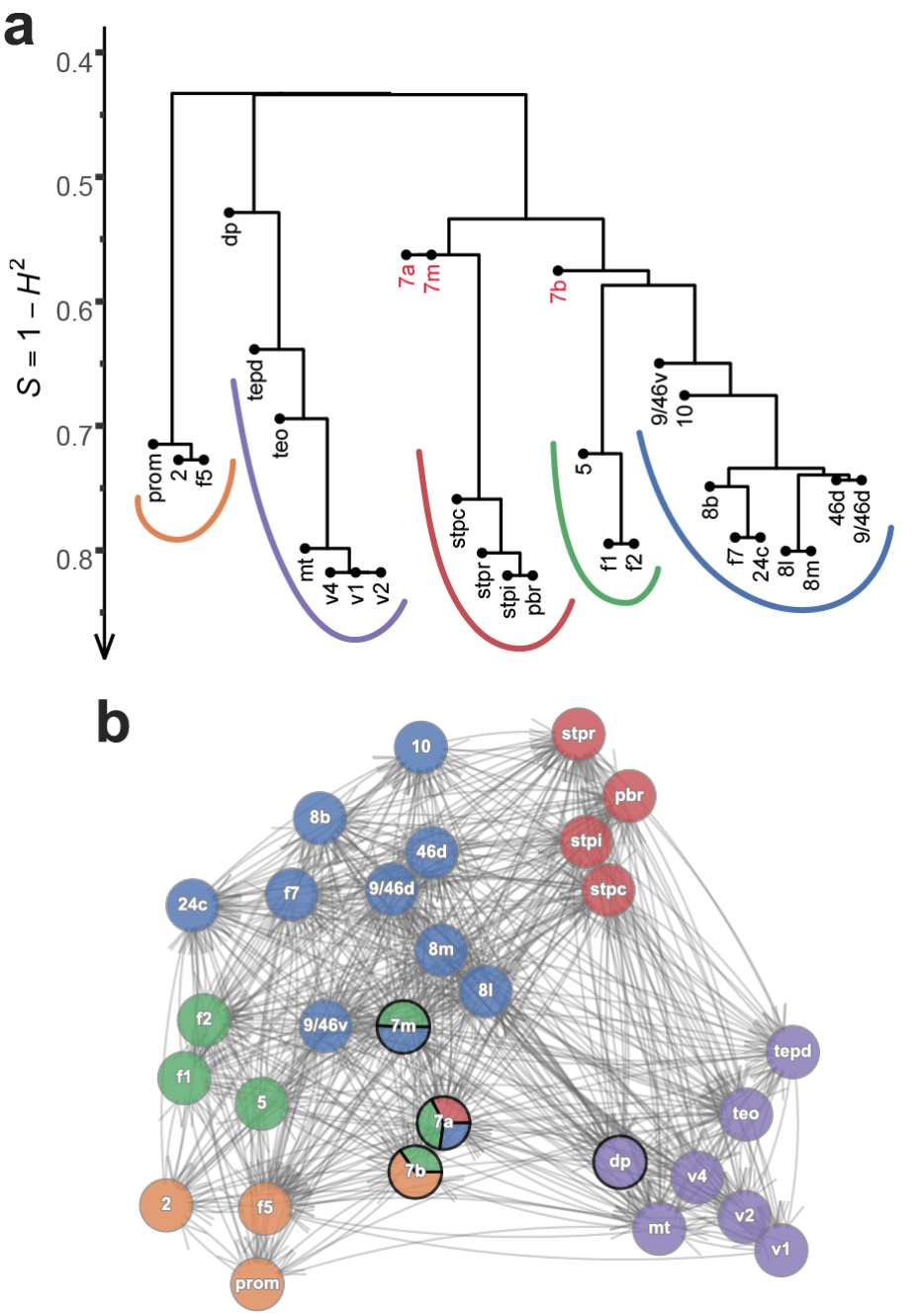

1260

Extended Data Fig. 2| Community analysis of the edge-complete network of a previous FLN macaque dataset with 29 injected areas (N. T. Markov *et al.*, 2014a). a, All the branches of this NCh correspond to one branch of **Fig. 3**d. This shows that the hierarchical community structure of the interareal cortical network is robust since 11 extra injections does not change substantially the structure already observed with 29. Red areas are the NOCs in **b**. **b**, At the optimal loop entropy partition, there are five node communities and three NOCs. Only area 7b is also classified as a NOC in the ECN with 40 injected areas. As expected, NOCs are more sensible to network changes. However, some are conserved and be present even in the final dataset, when all the areas have been injected.

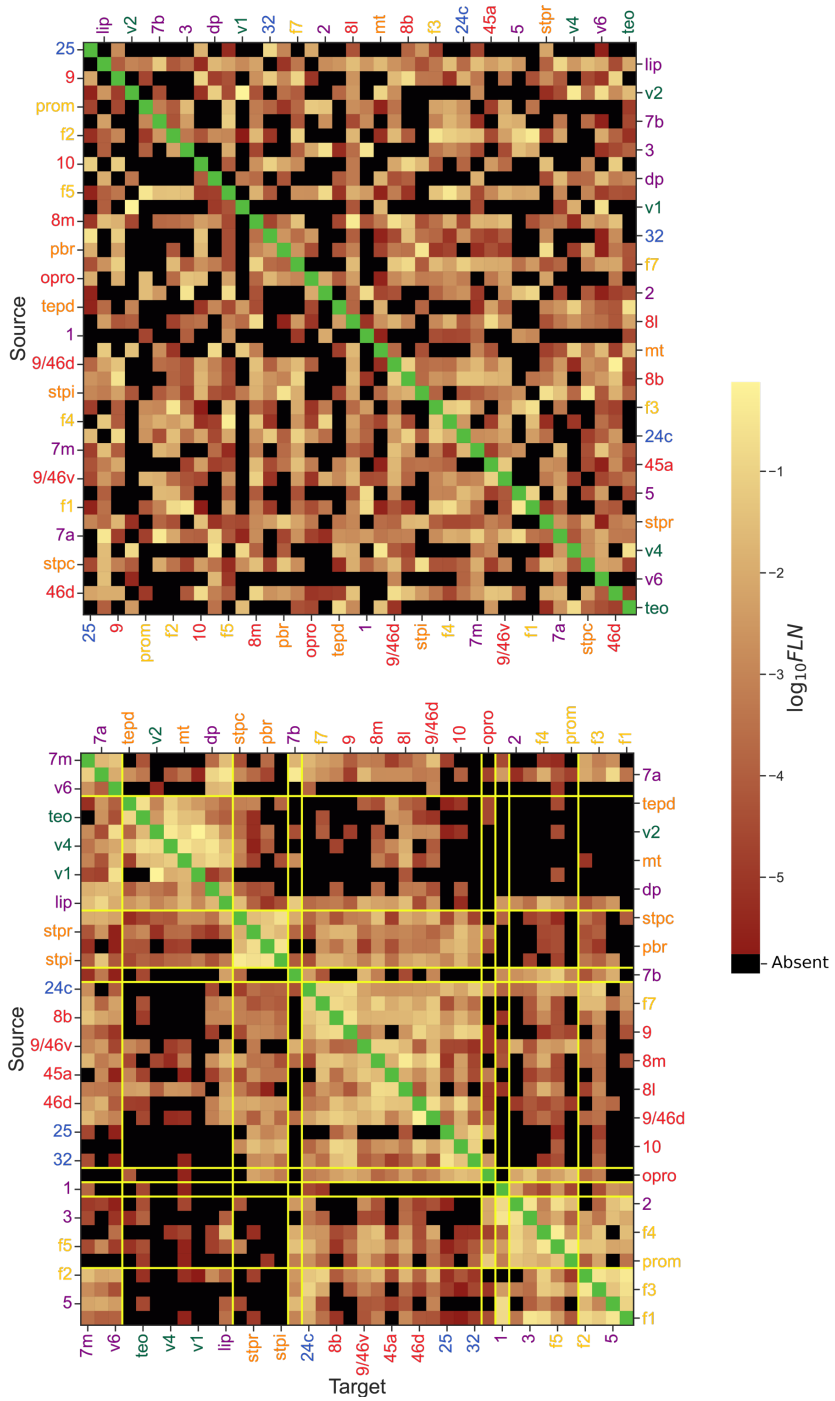

Extended Data Fig. 3| Connection strength heatmaps of the ECN. Rows and columns are arranged randomly in the top while organized following the order of the NCh in the bottom. Yellow vertical and horizontal lines show the borders between node communities at the optimal loop entropy level. Absent and intrinsic connections are colored in black and green, respectively. Without information about the network's community structure, it is challenging to distinguish it from a structureless random graph.

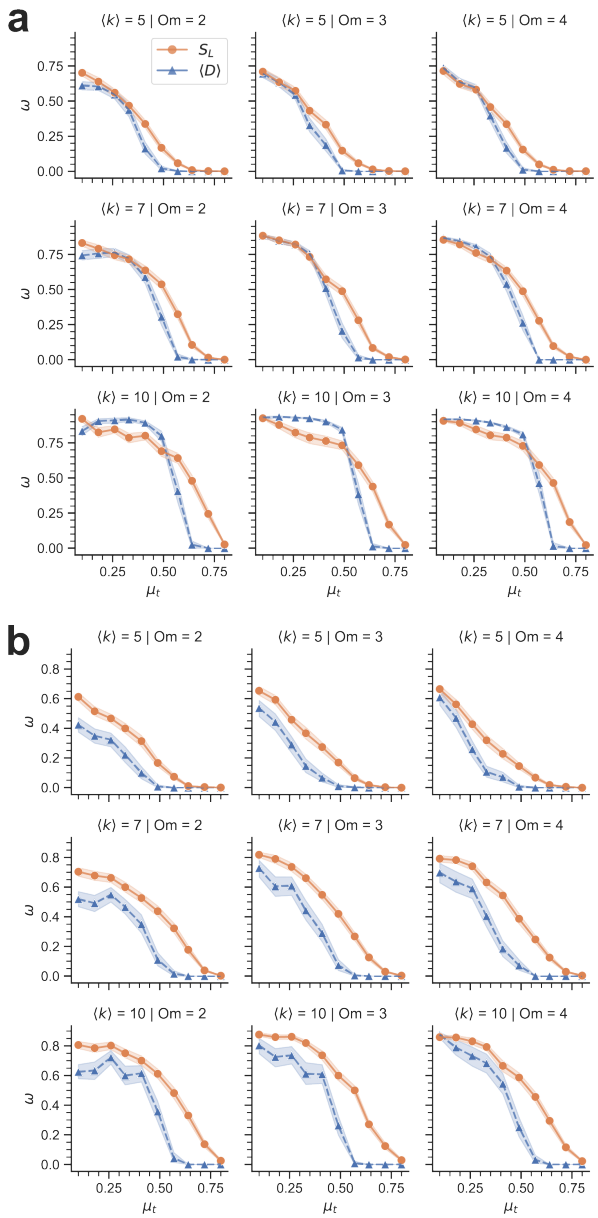

Extended Data Fig. 4| Algorithm validation. a-b, We used the LF benchmark (Lancichinetti and Fortunato, 2009) to generate weighted and directed random networks with ground-truth community structure, allowing some nodes to belong to more than one community. The networks have 100 nodes, 5% of them have 2, 3, or 4 overlapping community memberships (Om; columns). The average degree $\langle k \rangle$ of the networks is 5, 7, or 10 (rows). We varied the topology mixing parameter μ_t (see Methods section) from 0.1 to 0.8 in steps of 7/90 to assess the performance in networks from low to high complexity. Panel **a** and **b** are for networks where the maximum degree of a node is 30 and 50, respectively. For each point in the parameter space, we generated 100 instances, computed the node community hierarchy, found the optimal level using the average link community density $\langle D \rangle$ (see Methods section) and loop entropy S_L, assigned covers to any single-community node, and compared the predicted and ground-truth cover structures using the omega index ω. The analysis shows that S_L tends to perform better than the $\langle D \rangle$ in most cases, except for the last row of panel **a**, where due to the effect of creating networks with average degree close to the maximum degree, which itself is of low value (sparser network), there are few external links (between nodes participating in different communities), and in this case local density can be a more suitable community score. Markers and shades represent averages and one standard deviation region, respectively.

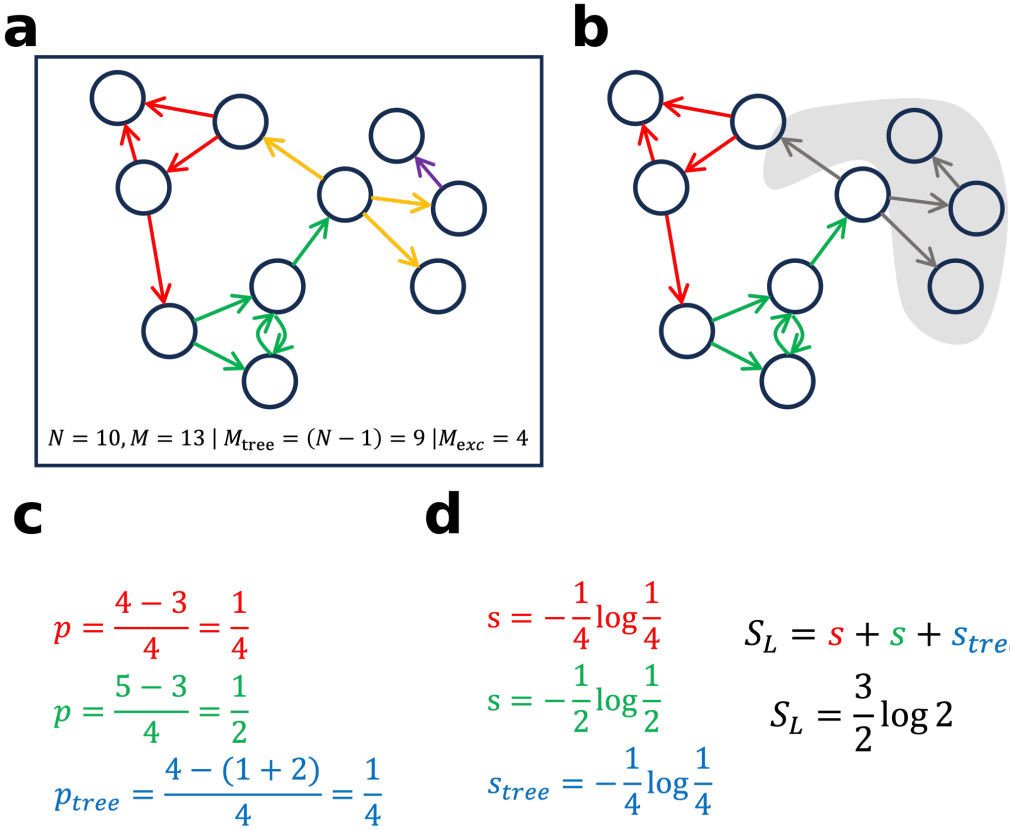

Extended Data Fig. 5| Loop entropy example. a, Toy network with 10 nodes and 13 directed links. Links are distributed in five link communities. The number of excess M_{exc} links of this network is four. **b,** The red and green link communities are the only ones that are not trees because their $M_{exc} > 0$. **c,** We compute the probability of sampling excess links in the red and blue green link communities and the normalization factor p_{tree}. **d,** Finally, the loop entropy S_L is simply the Shannon-Gibbs entropy of the excess-link probability distribution.

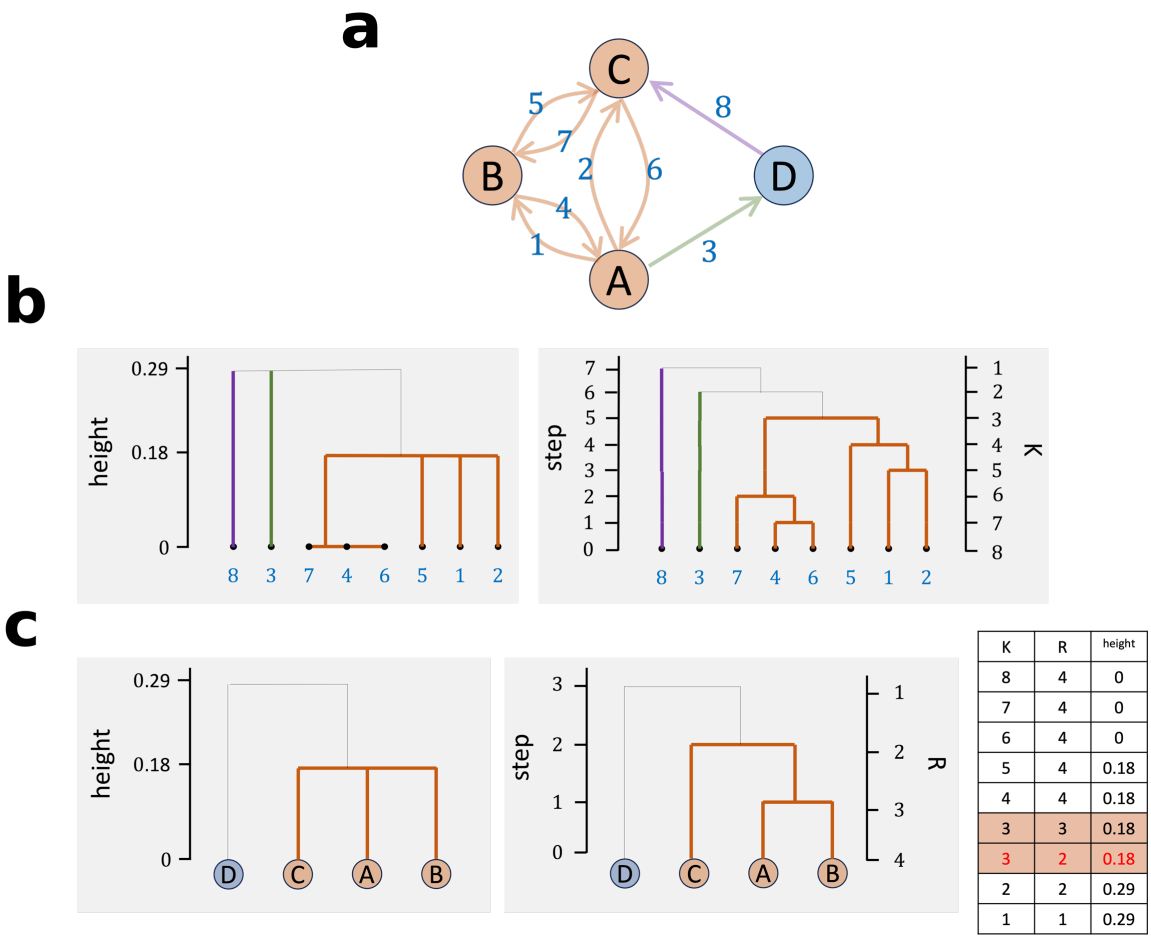

K	R	height
8	4	0
7	4	0
6	4	0
5	4	0.18
4	4	0.18
3	3	0.18
3	2	0.18
2	2	0.29
1	1	0.29

Extended Data Fig. 6| Finding a node-community hierarchy level from a link-community hierarchy level. a, Toy network with four nodes and eight directed links. Links are numbered and their colors represent link communities found at the optimal level. Node communities associated with that level are similarly colored. Node "D" is a single-node community. **b**, (left) LCh of the network where levels are written in terms of the threshold (height). **b**, (right) Same LCh but its levels have been separated by link merging step and number of link communities, K, as shown by the left and right vertical axis, respectively. Each node at the bottom is one link from the toy network. Branches show the progression of the link merging process, and thick colored ones represent different link communities. **c**, Same as **b**, but for the NCh. Hierarchy levels separated by (left) height; **c**, (center) node merging steps, and number of node communities, denoted by R. Thick colored branches are associated with the non-single node community. **c**, (right) By storing in a table the information of K, R, and height across the link merging process, we can find how many node communities R existed at any LCh level K. If there are more than one node merging event at a particular K, we select the one with lowest R.

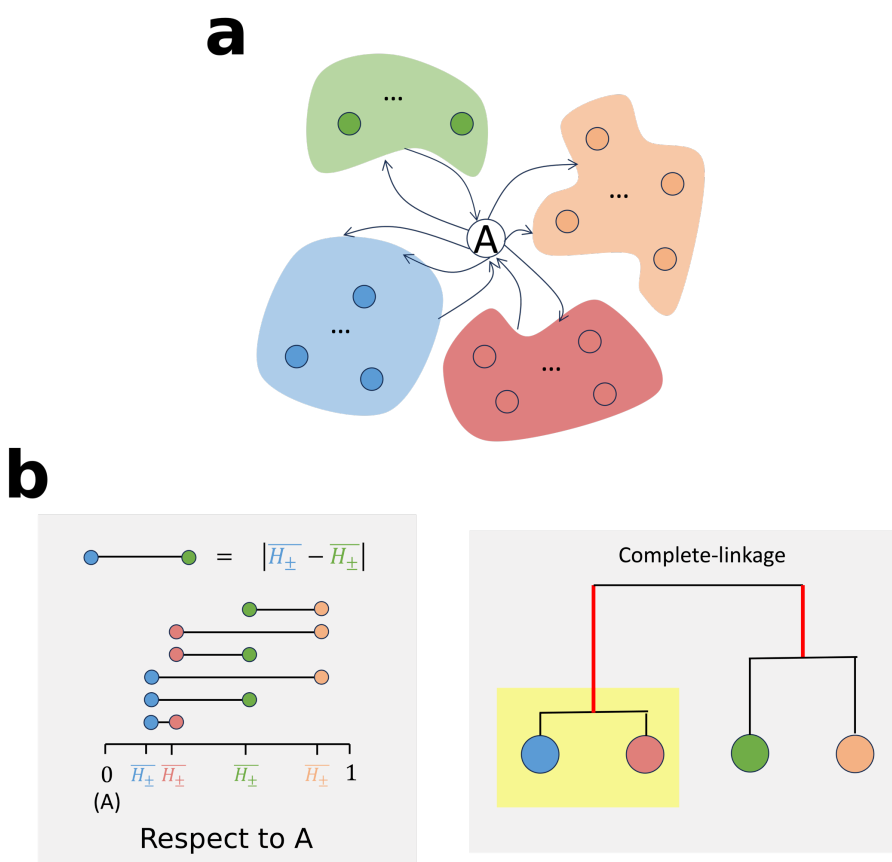

Extended Data Fig. 7| Cover assignment algorithm. a, In this illustration, node "A" is a single-node community, i.e., no other node in the network participates with "A" in the same node community. We want to assign to some of the existing non-single node communities, shown by colored shapes. **b**, (left) To that aim, for each directed neighborhood, the mean Hellinger distance ($\overline{H_{\pm}}$) between the single-node community and the nodes in each non-single node communities is computed. The distance represents the dissimilarity centroid (DC) between the single-node community and a non-single node community. Given that H is a metric, the relative difference between each $\overline{H_{\pm}}$ is computed and will satisfy the triangle inequality. (right) For each direction, the DCs are clustered using a hierarchical agglomeration algorithm with complete-linkage criterion, i.e., the dissimilarity between groups is the maximum dissimilarity between group's elements (Müllner, 2013), creating a DC hierarchy. The criterion is chosen since DCs are expected to associate with highly distinguishable clusters. To finish, the DC hierarchy is partitioned at the level before the largest dissimilarity threshold increment (thick red branches), and the single-node community receives the membership(s) of the DCs in the branch with the most similar DC.

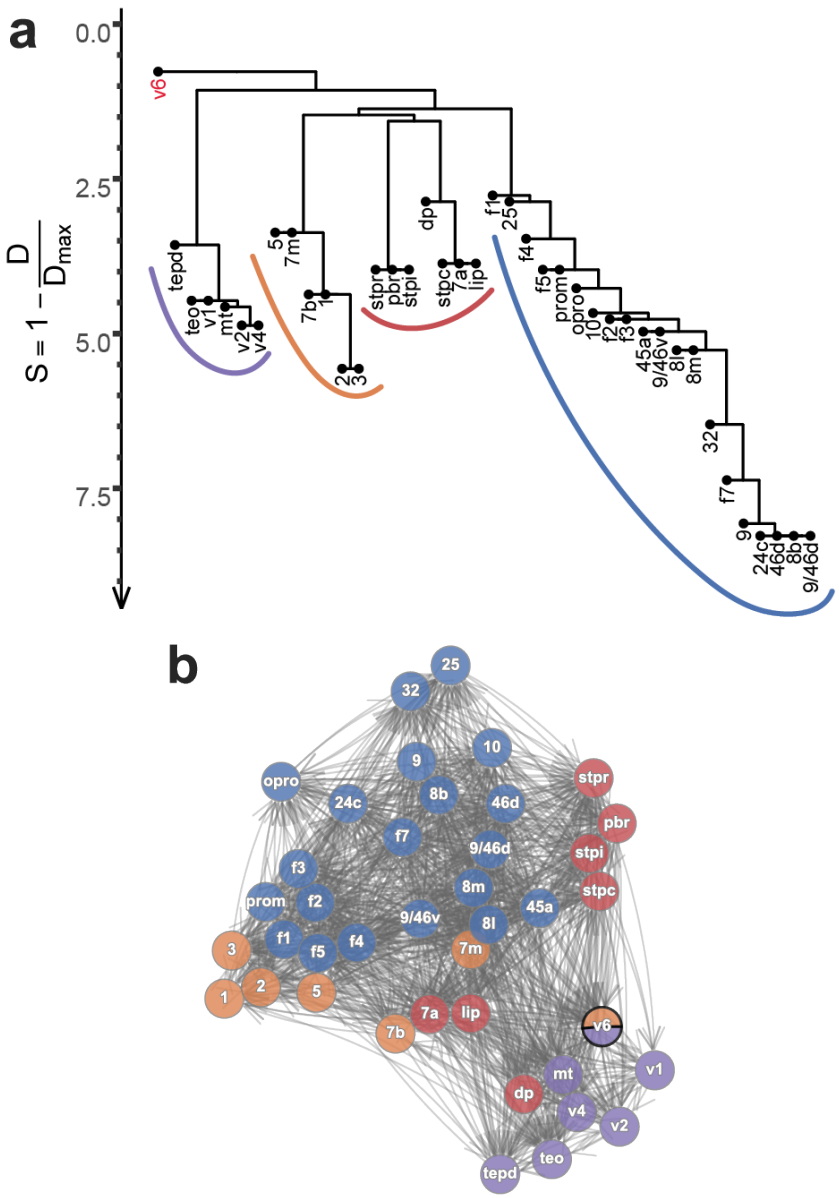

1267

Extended Data Fig. 8| Community analysis using interareal distance as dissimilarity measure. **a**, NCh derived by replacing areal similarities by one minus the interareal distance divided by the maximum whole brain interareal distance. There are some commonalities and differences with respect to the NCh using the Hellinger dissimilarity measure (H-NCh). For example, the visual ventral system, above the purple arc, is almost the same as in the H-NCh. However, the rest of the branches tend to differ. A marked discrepancy is seen in the branch above the blue arc, which consists of prefrontal areas, because it does not show any sub-branches, i.e., a lack of functional specialization. The red area V6 is a NOC in this model, in contrast with the H-NCh. **b**, At the optimal loop entropy level, four communities are found, which is less than the six shown in **Fig. 3**d. Additionally, the omega index of this partition and the one from data is $\omega = 0.48$, which is close to the value of the one for the EDR model (0.44), see **Fig. 5**a. This shows that besides the ventral visual system, the model does not reproduce well the expected functional components of the macaque ECN. Therefore, the interareal distance-based hierarchy encodes around 50% of the functional structure found with Hellinger distances.